

(NASA-CR-175848) FLUTTER ANALYSIS OF A
TUNED ROTOR WITH RIGID AND FLEXIBLE DISKS
(Massachusetts Inst. of Tech.) 76 p

N85-72934

Unclas
00/07 23423

FLUTTER ANALYSIS OF A TUNED ROTOR
WITH RIGID AND FLEXIBLE DISKS

by
John Dugundji

GT&PDL Report No. 146

July 1979



GAS TURBINE & PLASMA DYNAMICS LABORATORY
MASSACHUSETTS INSTITUTE OF TECHNOLOGY
CAMBRIDGE, MASSACHUSETTS

FLUTTER ANALYSIS OF A TUNED ROTOR
WITH RIGID AND FLEXIBLE DISKS

by
John Dugundji

GT&PDL Report No. 146

July 1979

ACKNOWLEDGEMENTS

The author would like to acknowledge helpful discussions with Prof. J. L. Kerrebrock and Mr. E. F. Crawley during the course of this work.

This research, carried out in the Gas Turbine Laboratory, M.I.T., was supported by NASA Lewis Research Center under Grant No. NSG-3079, "Research on Turbomachine Flutter". The NASA Technical Officer for this work was Dr. John J. Adamczyk.

ABSTRACT

The flutter behavior of a simple tuned rotor with a rigid and a flexible disk is reviewed.

In Part A, the rotor assembly is assumed to consist of a rigid disk with N uniform flexible blades attached around the circumference, so that the blades are coupled only by aerodynamic forces. Both traveling wave and standing wave flutter analyses are conducted, and are shown to be equivalent. The relations between traveling and standing wave air forces are described in detail. The standing wave analysis is shown to be more versatile for some applications than the simpler traveling wave analysis. Applications are made to pure bending flutter and pure torsion flutter of the rotor assembly. Comments are made on combined bending-torsion flutter.

In Part B, the rotor disk is assumed flexible and shrouds may be present. The blades are here coupled structurally as well as aerodynamically. The corresponding vibration and flutter behavior is examined.

TABLE OF CONTENTS

	<u>Page</u>
1. Introduction	8
PART A: Rigid Disk	9
2. Traveling Wave Analysis (Simple)	9
3. Traveling Wave Analysis (Alternate)	13
4. Relations between Traveling & Standing Waves	17
5. Standing Wave Analysis	22
6. Application to Bending Flutter	29
7. Application to Torsion Flutter	32
8. Combined Bending-Torsion Flutter	35
PART B: Flexible Disk	40
9. Description of Vibration Modes	40
10. Traveling Wave Analysis	44
11. Further Remarks on Flutter	52
12. Conclusions	57
References	58
Tables	59
Figures	64

NOMENCLATURE

A	complex aerodynamic force = $A_R + i A_I$
\bar{A}	nondimensional complex aerodynamic force = $\bar{A}_R + i \bar{A}_I$
a	real part of characteristic root, p
b	semichord = $c/2$
C	damping force for overall rotor mode
C_{Fq}, C_{Fa}	aerodynamic force and moment coefficients
C_{Mq}, C_{Ma}	" " " " "
c	damping force for blade
c	chord
F_j	blade force per unit length
f_j	total force on blade
f^D	disturbance force on rotor disk
h_0	modal deflection at elastic axis
I	moment of inertia of blade
i	$\sqrt{-1}$
K	stiffness for overall rotor mode
k	stiffness for blade
k	reduced frequency = $\omega b/V$
l	average span of blade
l_h, l_α	complex aerodynamic force coefficients
M	mass for overall rotor mode
\bar{M}_j	blade moment per unit length

NOMENCLATURE Continued

m	mass for blade
\overline{m}_j	total moment on blade
N	number of blades on rotor
n	number of nodal diameters in overall rotor mode
p	characteristic root = $a + i\omega$
q_c, q_s	generalized coordinates for a vibration mode
q_0, q_1, q_2	nondimensional generalized coordinates
R	radius of rotor
S	static unbalance of blade
s	gap between two rotor blades
T	kinetic energy
t	time
U	potential energy
V	velocity of flow at blade
w_j, w_0	displacements of blade
w_D, w_B	" " "
$\alpha_j, \alpha_0, \alpha_B$	twist angle of blade
α_c, α_s	modal twist about elastic axis
β	interblade phase angle = $n2\pi/N$
ζ_A	aerodynamic damping ratio
ζ_S	critical damping ratio of structure
η	location of elastic axis

NOMENCLATURE Continued

θ, θ_j	angular position relative to rotor.
$\bar{\theta}$	angular position relative to fixed space
μ	mass density ratio = $m/\pi p b^2 \ell$, = $2M/\pi p b^4 \ell N$
ξ	stagger angle
Ω	rotation speed of rotor
ρ	air density
ϕ	structural coupling angle
ω	frequency of oscillations
ω_n	natural frequency

PART A: RIGID DISK

Assume a balanced, tuned rotor with a rigid disk. Only aerodynamic coupling is possible between the blades. See Fig. 1. The traveling wave and standing wave flutter behavior of the above rotor system, will be investigated in Part A.

2. Traveling Wave Analysis (Simple)

The equations of motion for the tuned rotor on a rigid disk shown in Fig. 1 can be represented by $N = 23$ identical blade equations of the form,

$$m \ddot{w}_j + c \dot{w}_j + k w_j = f_j \quad (1)$$

$j = 1, 2, \dots, N$

where w_j represents the displacement of the j th blade at some reference section. Because the blades are mounted in a circular ring, one looks for traveling wave solutions of the form,

$$w_j = w_0 e^{i(\omega t + j\beta)} \quad (2)$$

where,

$$\theta_j = \frac{2\pi}{N} j \quad \text{blade location}$$

$$j\beta = n \frac{2\pi}{N} j \quad \text{angle of blade for } n \text{ nodal diams.}$$

hence,

$$\beta \equiv n \frac{2\pi}{N} \quad \text{interblade phase angle}$$

For the physical significance of Eq. (2), one takes the real part, i.e.,

$$\operatorname{Re} \{ w_j \} = w_0 \cos(\omega t + \beta j) \quad (2a)$$

This gives the instantaneous deflection of any blade j .

The airforces corresponding to Eq. (2) are represented as,

$$f_j = (A_R + i A_I) w_0 e^{i(\omega t + \beta j)} \quad (3)$$

These can be obtained theoretically or experimentally in cascade tunnels.

Placing the assumed solution Eq. (2) and corresponding airforces Eqs. (3) into

the basic Eq. (1) gives,

$$\begin{aligned} -\omega^2 m w_0 e^{i(\omega t + \beta j)} + i\omega c w_0 e^{i(\omega t + \beta j)} + k w_0 e^{i(\omega t + \beta j)} &= \\ &= (A_R + i A_I) w_0 e^{i(\omega t + \beta j)} \end{aligned}$$

$$\text{Real Eq.:} \quad -\omega^2 m + k - A_R = 0$$

(4)

$$\text{Imag. Eq.:} \quad \omega c - A_I = 0$$

The airforces A_R , A_I are functions of reduced frequency $\omega b/v$, gap to chord ratio s/c , interblade phase angle β , etc.

Flutter occurs when both Eqs. (4) are satisfied. From the real equation,

$$\omega^2 = \frac{k}{m} - \frac{A_R}{m} \quad (4a)$$

Usually $A_R \ll k$ and hence the flutter frequency will not be altered much from the measured natural frequency, ω_n . From the imaginary equation, one has the conditions,

$$\text{If, } \omega c - A_I = 0 \rightarrow \text{Flutter,} \quad (4b)$$

$$\text{If, } \omega c - A_I > 0 \rightarrow \text{Stable} \quad (4c)$$

$$\text{If, } \omega c - A_I < 0 \rightarrow \text{Unstable} \quad (4d)$$

Equation (4b) corresponds to the mechanical damping + aerodynamic damping = 0, while (4c) and (4d) correspond to the total damping being positive or negative.

All interblade phase angles β should be investigated. The values of β that make $\omega c - A_I < 0$ are considered unstable. The value of β that makes $\omega c - A_I$ most negative is the flutter that will occur first. Then, the flutter mode would be given by

$$n = \frac{N}{2\pi} \beta \quad (4e)$$

where n takes on integer values only. This results in a traveling wave with n nodal diameters, which rotates at a speed ω/n . See Eq. (2a). The aerodynamic coupling picks out the most unstable traveling wave mode n for the rotor assembly.

NOTE: One can always rewrite the aerodynamic force,

$$f_j = (A_R + i A_I) w_o e^{i(\omega t + \beta j)} \quad (3)$$

in the form,

$$f_j = A_R w_j + \frac{A_I}{\omega} \dot{w}_j \quad (5)$$

since, for solutions of form, $w_j = w_o e^{i(\omega t + \beta j)}$, one has

$$f_j = A_R w_o e^{i(\omega t + \beta j)} + \frac{A_I}{\omega} i \omega w_o e^{i(\omega t + \beta j)} \quad (5a)$$

Hence, it is seen that the damping coefficient A_I/ω , is the key coefficient to be examined. Positive values of A_I can lead to instability. Because of interference from other blades, this A_I can become positive and large. For isolated blades, A_I is usually negative (stable).

The type of flutter described by Eqs. (4) can be designated as, "Single Degree of Freedom, Traveling Wave Flutter." It represents a common type of flutter analysis for rotor blades.

3. Traveling Wave Analysis (Alternate)

For many analyses, it is often preferable to describe the system in terms of the 2 overall standing wave disk modes, $\cos \beta j$ and $\sin \beta j$, corresponding to a given number of nodal diameters n .

$$W_j = q_c \cos \beta j + q_s \sin \beta j \quad (6)$$

where,

$q_c, q_s \rightarrow$ generalized coordinates

$\cos \beta j, \sin \beta j \rightarrow$ disk modes for n^{th} nodal diameter

$\beta \equiv n \frac{2\pi}{N} \rightarrow$ interblade phase angle

Equation (6) is a standing wave representation of the blade motions, in contrast to the previous traveling wave representation, Eq. (2).

To obtain modal equations for q_c and q_s , use Rayleigh-Ritz Method.

Kinetic energy is,

$$\begin{aligned} T &= \frac{1}{2} \sum_{j=1}^{23} m_j \dot{W}_j^2 = \frac{1}{2} \sum_{j=1}^{23} m_j \left[\dot{q}_c \cos \beta j + \dot{q}_s \sin \beta j \right]^2 \\ &= \frac{1}{2} m \left[\dot{q}_c^2 \sum_{j=1}^{23} \cos^2 \beta j + \dot{q}_s^2 \sum_{j=1}^{23} \sin^2 \beta j + 2 \dot{q}_s \dot{q}_c \sum_{j=1}^{23} \sin \beta j \cos \beta j \right] \end{aligned}$$

where $m_j = m = \text{same for all blades}$. Now, the following useful trigonometric summations are introduced which are valid for $N \geq 3$,

$$\sum_{j=1}^N \cos^2 \beta_j = \sum_{j=1}^N \sin^2 \beta_j = \frac{N}{2} \quad (7)$$

$$\sum_{j=1}^N \sin \beta_j \cos \beta_j = 0$$

Using these, the kinetic energy becomes,

$$T = \frac{1}{2} M \dot{q}_c^2 + \frac{1}{2} M \dot{q}_s^2$$

where $M \equiv mN/2$. Next, the potential energy of the system is,

$$U = \frac{1}{2} \sum_{j=1}^{23} k_j w_j^2 = \frac{1}{2} \sum_{j=1}^{23} k_j [q_c \cos \beta_j + q_s \sin \beta_j]^2$$

$$= \frac{1}{2} K q_c^2 + \frac{1}{2} K q_s^2$$

where $K \equiv kN/2$. The incremental work of the external forces acting on the system is,

$$\begin{aligned} \delta W &= \sum_{j=1}^{23} [f_j - c_j \dot{w}_j] \delta w_j \\ &= \sum_{j=1}^{23} [f_j - c_j \dot{q}_c \cos \beta_j - c_j \dot{q}_s \sin \beta_j] [\delta q_c \cos \beta_j + \delta q_s \sin \beta_j] \\ &= \sum_{j=1}^{23} [f_j \cos \beta_j - c_j \dot{q}_c \cos^2 \beta_j - c_j \dot{q}_s \sin \beta_j \cos \beta_j] \delta q_c \\ &\quad + \sum_{j=1}^{23} [f_j \sin \beta_j - c_j \dot{q}_c \cos \beta_j \sin \beta_j - c_j \dot{q}_s \sin^2 \beta_j] \delta q_s \end{aligned}$$

Introducing the trigonometric summations, Eqs. (7), gives,

$$\begin{aligned} \delta W = & \left[\sum_{j=1}^{23} f_j \cos \beta_j - c \frac{N}{2} \dot{q}_c \right] \delta q_c \\ & + \left[\sum_{j=1}^{23} f_j \sin \beta_j - c \frac{N}{2} \dot{q}_s \right] \delta q_s = \sum_{i=1}^2 Q_i \delta q_i \end{aligned}$$

Placing T , U , and Q_i into Lagrange's equations,

$$\frac{d}{dt} \left(\frac{\partial T}{\partial \dot{q}_i} \right) - \frac{\partial T}{\partial q_i} + \frac{\partial U}{\partial q_i} = Q_i$$

gives finally the 2 equations of motion for q_c and q_s defined in Eq. (6) as,

$$\begin{aligned} M \ddot{q}_c + C \dot{q}_c + K q_c &= \sum_{j=1}^{23} f_j \cos \beta_j \\ M \ddot{q}_s + C \dot{q}_s + K q_s &= \sum_{j=1}^{23} f_j \sin \beta_j \end{aligned} \quad (8)$$

where, $M = mN/2$, $C = cN/2$, $K = kN/2$ represent parameters for the n th circumferential mode, and $\beta = n2\pi/N$ is the interblade phase angle.

To obtain traveling wave solutions for Eq. (8), multiply 1st equation by $\cos \beta k$, 2nd equation by $\sin \beta k$, and add to give,

$$\begin{aligned} M \ddot{w}_k + C \dot{w}_k + K w_k &= \\ &= \cos \beta k \sum_{j=1}^{23} f_j \cos \beta_j + \sin \beta k \sum_{j=1}^{23} f_j \sin \beta_j \end{aligned}$$

Then look for traveling wave solutions of form,

$$w_k = w_0 e^{i(\omega t + \beta k)} \quad (10)$$

Corresponding air forces are represented as,

$$f_j = (A_R + i A_I) w_0 e^{i(\omega t + \beta j)} \quad (11)$$

Placing Eqs. (10) and (11) into Eq. (9) gives,

$$\begin{aligned} -\omega^2 M w_0 e^{i(\omega t + \beta k)} + i\omega w_0 C e^{i(\omega t + \beta k)} + K w_0 e^{i(\omega t + \beta k)} = \\ = (A_R + i A_I) w_0 e^{i\omega t} \left\{ \cos \beta k \sum_{j=1}^{23} \cos \beta j (\cos \beta j + i \sin \beta j) \right. \\ \left. + \sin \beta k \sum_{j=1}^{23} \sin \beta j (\cos \beta j + i \sin \beta j) \right\} \end{aligned}$$

Introducing the previous relations of Eqs. (7) into the R.H.S. of these equations gives,

$$\text{R.H.S.} = (A_R + i A_I) w_0 e^{i\omega t} \frac{N}{2} (\cos \beta k + i \sin \beta k)$$

Placing back into previous equations gives

$$\begin{aligned} -\omega^2 M w_0 e^{i(\omega t + \beta k)} + i\omega C w_0 e^{i(\omega t + \beta k)} + K w_0 e^{i(\omega t + \beta k)} = \\ = \frac{N}{2} (A_R + i A_I) w_0 e^{i(\omega t + \beta k)} \end{aligned}$$

$$\text{Real Eq.:} \quad -\omega^2 M + K - \frac{N}{2} A_R = 0 \quad (12)$$

$$\text{Imag. Eq.:} \quad \omega C - \frac{N}{2} A_I = 0$$

These are the same equations as the previous Eqs. (4), since $M = mN/2$, $K = \text{etc.}$

4. Relations between Traveling and Standing Waves

Given the traveling wave deflection,

$$w_j = w_0 e^{i(\omega t + \beta j)} \quad j = 1, 2, 3, \dots, N \quad (2)$$

which physically can be represented by its real part as,

$$\begin{aligned} \text{Re} \{w_j\} &= w_0 \cos(\omega t + \beta j) \\ w_j &= w_0 \cos \beta j \cos \omega t - w_0 \sin \beta j \sin \omega t \end{aligned} \quad (13)$$

The corresponding airforces are

$$f_j = (A_R + iA_I) w_0 e^{i(\omega t + \beta j)} \quad (3)$$

$$\begin{aligned} \text{Re} \{f_j\} &= A_R w_0 \cos(\omega t + \beta j) - A_I w_0 \sin(\omega t + \beta j) \\ f_j &= \cos \beta j [A_R w_0 \cos \omega t - A_I w_0 \sin \omega t] \\ &\quad + \sin \beta j [-A_I w_0 \cos \omega t - A_R w_0 \sin \omega t] \end{aligned} \quad (14)$$

The A_R , A_I are obtained from theoretical or experimental analyses of cascades with interblade phase angles, β .

Next, add 2 traveling waves of amplitude $w_0/2$, traveling in opposite directions ($+\beta$ and $-\beta$)

$$w_j = \frac{w_0}{2} \left[\cos \beta_j \sin \omega t - \sin \beta_j \sin \omega t \right] \\ + \frac{w_0}{2} \left[\cos \beta_j \cos \omega t + \sin \beta_j \sin \omega t \right]$$

$$w_j = w_0 \cos \beta_j \cos \omega t \quad (15)$$

The corresponding airforces f_j are

$$f_j = \cos \beta_j \left[A_R^+ \frac{w_0}{2} \cos \omega t - A_I^+ \frac{w_0}{2} \sin \omega t \right] \\ + \sin \beta_j \left[-A_I^+ \frac{w_0}{2} \cos \omega t - A_R^+ \frac{w_0}{2} \sin \omega t \right] \\ + \cos \beta_j \left[A_R^- \frac{w_0}{2} \cos \omega t - A_I^- \frac{w_0}{2} \sin \omega t \right] \\ - \sin \beta_j \left[-A_I^- \frac{w_0}{2} \cos \omega t - A_R^- \frac{w_0}{2} \sin \omega t \right]$$

Gathering together gives,

$$f_j = \cos \beta_j \left[A_1 w_0 \cos \omega t - A_2 w_0 \sin \omega t \right] \\ + \sin \beta_j \left[-A_4 w_0 \cos \omega t - A_3 w_0 \sin \omega t \right] \quad (16)$$

where the coefficients A_1, A_2, A_3, A_4 are related to the traveling wave coefficients A_R and A_I

$$\begin{aligned} A_1 &= \frac{A_R^+ + A_R^-}{2} & A_2 &= \frac{A_I^+ + A_I^-}{2} \\ A_3 &= \frac{A_R^+ - A_R^-}{2} & A_4 &= \frac{A_I^+ - A_I^-}{2} \end{aligned} \quad (17)$$

A sketch of the standing wave oscillation pattern is shown in Fig. 2.

Similarly, taking two traveling waves of amplitude $w_0/2$ traveling in opposite directions and subtracting gives,

$$\begin{aligned} w_j &= -\frac{w_0}{2} \left[\cancel{\cos \beta_j} \cos \omega t - \sin \beta_j \sin \omega t \right] \\ &\quad + \frac{w_0}{2} \left[\cancel{\cos \beta_j} \cos \omega t + \sin \beta_j \sin \omega t \right] \\ w_j &= w_0 \sin \beta_j \sin \omega t \end{aligned} \quad (18)$$

The corresponding airforces f_j becomes,

$$\begin{aligned} f_j &= \cos \beta_j \left[-A_R^+ \frac{w_0}{2} \cos \omega t + A_I^+ \frac{w_0}{2} \sin \omega t \right] \\ &\quad + \sin \beta_j \left[+A_I^+ \frac{w_0}{2} \cos \omega t + A_R^+ \frac{w_0}{2} \sin \omega t \right] \\ &\quad + \cos \beta_j \left[A_R^- \frac{w_0}{2} \cos \omega t - A_I^- \frac{w_0}{2} \sin \omega t \right] \\ &\quad - \sin \beta_j \left[-A_I^- \frac{w_0}{2} \cos \omega t - A_R^- \frac{w_0}{2} \sin \omega t \right] \end{aligned}$$

Gathering together gives,

$$f_j = \cos \beta_j \left[-A_3 w_0 \cos \omega t + A_4 w_0 \sin \omega t \right] + \sin \beta_j \left[A_2 w_0 \cos \omega t + A_1 w_0 \sin \omega t \right] \quad (19)$$

where A_1, A_2, A_3, A_4 are as defined before by Eqs. (17).

NOTE: One can rewrite Eqs. (15) and (16) as

$$w_j = q_c \cos \beta_j \quad (20)$$

$$f_j = \cos \beta_j \left[A_1 q_c + \frac{A_2}{\omega} \dot{q}_c \right] + \sin \beta_j \left[-A_4 q_c + \frac{A_3}{\omega} \dot{q}_c \right] \quad (21)$$

since, for solutions of form $q_c = w_0 \cos \omega t$, above reduce to Eqs. (15) and (16).

Similarly, one can rewrite Eqs. (18) and (19) as,

$$w_j = q_s \sin \beta_j \quad (22)$$

$$f_j = \cos \beta_j \left[A_4 q_s - \frac{A_3}{\omega} \dot{q}_s \right] + \sin \beta_j \left[A_1 q_s + \frac{A_2}{\omega} \dot{q}_s \right] \quad (23)$$

since for solutions of form $q_s = w_0 \sin \omega t$, above reduces to Eqs. (18) and (19).

Finally, to summarize the results of this section, one can represent the deflections and airforces in either of two forms:

(a) Traveling Wave representation,

$$w_j = w_0 e^{i(\omega t + \beta j)} \quad (2)$$

$$f_j = (A_R + i A_I) w_0 e^{i(\omega t + \beta j)} \quad (3)$$

(b) Standing Wave representation,

$$w_j = q_c \cos \beta j + q_s \sin \beta j \quad (24)$$

$$\begin{aligned} f_j = \cos \beta j & \left[\frac{A_2}{\omega} \dot{q}_c + A_1 q_c - \frac{A_3}{\omega} \dot{q}_s + A_4 q_s \right] \\ & + \sin \beta j \left[\frac{A_3}{\omega} \dot{q}_c - A_4 q_c + \frac{A_2}{\omega} \dot{q}_s + A_1 q_s \right] \end{aligned} \quad (25)$$

The standing wave coefficients A_1, A_2, A_3, A_4 are related to the traveling wave coefficients A_R and A_I through Eqs. (17).

5. Standing Wave Analysis

It is of interest to apply a conventional standing wave modal analysis to describe the instability mechanisms described previously by the traveling wave analysis. To this end, one describes the blade deflection, as in Section 3, by the two overall disk modes,

$$w_j = q_c \cos \beta j + q_s \sin \beta j \quad (6)$$

The corresponding equations of motion for the two coordinates q_c and q_s were derived in Section 3 as,

$$\begin{aligned} M \ddot{q}_c + C \dot{q}_c + K q_c &= \sum_{j=1}^{23} f_j \cos \beta j \\ M \ddot{q}_s + C \dot{q}_s + K q_s &= \sum_{j=1}^{23} f_j \sin \beta j \end{aligned} \quad (8)$$

where M , C , K , are the overall mass, damping, and stiffness of the n^{th} circumferential disk mode, and $\beta = n2\pi/N$ is the interblade phase angle.

The aerodynamic forces f_j corresponding to the deflection pattern Eq. (6) was given in Section 4 by Eq. (25). Placing this f_j into Eq. (8) gives

$$\begin{aligned} M \ddot{q}_c + C \dot{q}_c + K q_c &= \sum_{j=1}^{23} (\cos \beta j)^2 \left[\frac{A_2}{\omega} \dot{q}_c + A_1 q_c - \frac{A_3}{\omega} \dot{q}_s + A_4 q_s \right] \\ &+ \sum_{j=1}^{23} \cos \beta j \sin \beta j \left[\frac{A_3}{\omega} \dot{q}_c - A_4 q_c + \frac{A_2}{\omega} \dot{q}_s + A_1 q_s \right] \\ M \ddot{q}_s + C \dot{q}_s + K q_s &= \sum_{j=1}^{23} \sin \beta j \cos \beta j \left[\frac{A_2}{\omega} \dot{q}_c + A_1 q_c - \frac{A_3}{\omega} \dot{q}_s + A_4 q_s \right] \\ &+ \sum_{j=1}^{23} (\sin \beta j)^2 \left[\frac{A_3}{\omega} \dot{q}_c - A_4 q_c + \frac{A_2}{\omega} \dot{q}_s + A_1 q_s \right] \end{aligned}$$

Making use of the trigonometric summations Eqs. (7) and noting that $M = mN/2$, $C = cN/2$, $K = kN/2$ where m , c , k are the effective mass, damping and stiffness of a single blade, the above equations reduce to,

$$\begin{aligned} m \ddot{q}_c + \left(c - \frac{A_2}{\omega}\right) \dot{q}_c + (k - A_1) q_c + \frac{A_3}{\omega} \dot{q}_s - A_4 q_s &= 0 \\ -\frac{A_3}{\omega} \dot{q}_c + A_4 q_c + m \ddot{q}_s + \left(c - \frac{A_2}{\omega}\right) \dot{q}_s + (k - A_1) q_s &= 0 \end{aligned} \quad (26)$$

These equations represent a familiar gyroscopically-coupled system. Such equations occur for many rotating shaft and critical speed problems.

The stability of these equations can be investigated in the standard manner by looking for solutions of the form e^{pt} . The aerodynamic coefficients A_1 , A_2 , A_3 , A_4 are related to the traveling wave coefficients A_R and A_I through Eqs. (17), and are functions of frequency $\omega b/V$, inter-blade phase angle β , and other parameters. It is to be noted that A_3 and A_4 are important coupling parameters in these equations. If $A_3 = A_4 = 0$, which would occur if $A_R^+ = A_R^-$ and $A_I^+ = A_I^-$, the equations uncouple. Simple standing wave solutions for q_c and for q_s are then possible.

The general solution of Eqs. (26) can be found by assuming $q_c = \bar{q}_c e^{pt}$ and $q_s = \bar{q}_s e^{pt}$. These equations then become,

$$\begin{bmatrix} m p^2 + \left(c - \frac{A_2}{\omega}\right) p + (k - A_1) & \frac{A_3}{\omega} p - A_4 \\ -\frac{A_3}{\omega} p + A_4 & m p^2 + \left(c - \frac{A_2}{\omega}\right) p + (k - A_1) \end{bmatrix} \begin{Bmatrix} \bar{q}_c \\ \bar{q}_s \end{Bmatrix} = 0 \quad (27)$$

The characteristic determinant becomes,

$$m^2 p^4 + \left[2m \left(c - \frac{A_2}{\omega} \right) \right] p^3 + \left[\left(c - \frac{A_2}{\omega} \right)^2 + 2m(k_2 - A_1) + \left(\frac{A_3}{\omega} \right)^2 \right] p^2 + \left[2 \left(c - \frac{A_2}{\omega} \right) (k_2 - A_1) - 2 \frac{A_3 A_4}{\omega} \right] p + \left[(k_2 - A_1)^2 + A_4^2 \right] = 0 \quad (28)$$

One solves the above Eq. (28) for the four roots, p_i . Dynamic instability is present if any root p_i has a positive real part. The associated mode shape for any given root, $p_i = a + i\omega$, is,

$$\begin{aligned} \bar{q}_c &= 1 \\ \bar{q}_s &= \frac{m p^2 + \left(c - \frac{A_2}{\omega} \right) + (k_2 - A_1)}{-\frac{A_3}{\omega} p + A_4} \end{aligned} \quad (29)$$

The corresponding deflection shape is,

$$w_j = 1 e^{pt} \cos \beta j + \bar{q}_s e^{pt} \sin \beta j \quad (30)$$

For the actual physical deflection, one takes the real part of above, where it is understood that both p and \bar{q}_s may be complex, i.e., the $p = a + i\omega$ and $\bar{q}_s = \bar{q}_{sR} + i \bar{q}_{sI}$. This will then result in the actual deflection shape for the j^{th} blade as,

$$\begin{aligned} w_j &= \left\{ \cos \omega t \cos \beta j + (\bar{q}_{sR} \cos \omega t - \bar{q}_{sI} \sin \omega t) \sin \beta j \right\} e^{at} \\ &= \left\{ \cos (\omega t + \beta j) + [(1 - \bar{q}_{sI}) \sin \omega t + \bar{q}_{sR} \cos \omega t] \sin \beta j \right\} e^{at} \end{aligned} \quad (30)$$

The above response w_j corresponding to the given root $p_i = a + i\omega$, indicates both traveling and standing waves are generally present in the resultant motion. Note, that responses such that $a = 0$, $\bar{q}_{SR} = 0$, $\bar{q}_{SI} = 1$ will represent pure undamped traveling waves.

For finding the Flutter Speed only, rather than the general transient response of Eqs. (26), one seeks solutions where the roots p_i are pure imaginary, i.e., $p = i\omega$. This gives the borderline between decaying and amplifying oscillations. In Eqs. (26) one assumes solutions of the form,

$$\begin{aligned} q_c &= w_0 e^{i\omega t} \\ q_s &= i w_0 e^{i\omega t} \end{aligned} \quad (31)$$

Placing these into Eqs. (26) gives

$$-\omega^2 m + \left(c - \frac{A_2}{\omega}\right) i\omega + (k - A_1) - A_3 - i A_4 = 0 \quad (32)$$

$$-i A_3 + A_4 - i \omega^2 m - \left(c - \frac{A_2}{\omega}\right) \omega + i (k - A_1) = 0 \quad (33)$$

Dividing Eq. (33) by i gives exactly the same equation as Eq. (32).

Hence the assumed solution form, Eqs. (31), is a solution of the Eqs. (26) provided the real part and imaginary parts of Eq. (32) are satisfied, i.e.,

$$\begin{aligned}
 \text{Real Eq.:} \quad & -\omega^2 m + k \underbrace{-A_1 - A_3}_{= -A_R^+} = 0 \\
 \text{Imag. Eq.:} \quad & \omega_c c \underbrace{-A_2 - A_4}_{= -A_I^+} = 0
 \end{aligned} \tag{34}$$

This is exactly the same criterion as Eq. (4), which was found previously by the traveling wave analysis. The corresponding deflection shape is,

$$W_j = W_0 e^{i\omega t} \cos \beta j + i W_0 e^{i\omega t} \sin \beta j \tag{35}$$

Taking the real part of the above, gives the physical deflection shape as,

$$\begin{aligned}
 W_j &= W_0 \cos \omega t \cos \beta j - W_0 \sin \omega t \sin \beta j \\
 &= W_0 \cos (\omega t + \beta j)
 \end{aligned} \tag{36}$$

This represents a pure traveling wave as given by Eqs. (2a) and (2).

Thus it is seen that the standing wave analysis gives the same results as the traveling wave analysis.

The standing wave analysis, although somewhat more involved than the simpler traveling wave analysis described earlier in Sections 2 and 3, has certain advantages for some problems.

- (1) If 2 modes are not exactly the same (i.e., split),

$$\begin{aligned} M_c \ddot{q}_c + C_c \dot{q}_c + K_c q_c &= \dots \\ M_s \ddot{q}_s + C_s \dot{q}_s + K_s q_s &= \dots \end{aligned} \quad (37)$$

one will still be able to get flutter solutions, only now,

$$\bar{q}_s \neq i \bar{q}_c \quad (38)$$

This gives combined traveling and standing wave solutions at flutter.

- (2) One can readily incorporate Forced Vibrations into these equations as follows,

$$\begin{aligned} M_c \ddot{q}_c + C_c \dot{q}_c + K_c q_c &= \sum_{j=1}^{23} (f_j^{\text{aero}} + f_j^D) \cos \beta_j \\ M_s \ddot{q}_s + C_s \dot{q}_s + K_s q_s &= \sum_{j=1}^{23} (f_j^{\text{aero}} + f_j^D) \sin \beta_j \end{aligned} \quad (39)$$

where f_j^{aero} represent the previous aerodynamic forces which depend on the blade motions q_c , \dot{q}_c , q_s , \dot{q}_s , and f_j^D are the disturbance forces that depend on time, t . The homogeneous solution of the above equations ($f_j^D = 0$) gives the previous flutter solutions. The particular solution ($f_j^D \neq 0$) gives the forced

response including the aerodynamic damping from the f_j^{aero} . The forcing function f_j^D often arises from a steady, but non-uniformly distributed, entering flow field around the disk causing a force

$$f^D(\bar{\theta}) = f_{cm} \cos m\bar{\theta} + f_{sm} \sin m\bar{\theta} \quad (40)$$

on the rotor disk stage. In the above, $\bar{\theta}$ represents position relative to fixed space. See Fig. 3. The moving j^{th} blade would then experience a force,

$$f_j^D = f_{cm} \cos m(\theta_j - \Omega t) + f_{sm} \sin m(\theta_j - \Omega t) \quad (41)$$

where $\theta_j = 2\pi j/N$. The above could then be placed into Eqs. (39) to obtain the forced response of the rotor system.

- (3) There is the eventual possibility of using the standing wave analysis to include stand motion, bearing motion, shaft flexibility, whirl effects, etc., into a combined aeroelastic and mechanical stability analysis of the rotor system.

6. Application to Bending Flutter

The pure bending flutter of a rotor disk will be examined, using the simpler traveling wave theory described in Section 2. The geometrical layout of the rotor stage is shown in Fig. 4, and the blades are assumed to deform in pure bending motion only. The airforces will be expressed in terms of Whitehead's 2-dimensional, incompressible cascade theory given in Ref. 4.

The aerodynamic force per unit span on the j^{th} blade of a cascade is given by Whitehead as,

$$\begin{aligned} F_j &= \pi \rho V c i \omega w_0 C_{Fq} e^{i(\omega t + \beta j)} \\ &= \pi \rho \omega^2 b^2 \left(\frac{2i C_{Fq}}{k} \right) w_0 e^{i(\omega t + \beta j)} \end{aligned} \quad (42)$$

where b = semichord, $k = \omega b/V$ is the reduced frequency, and C_{Fq} is a nondimensional complex coefficient depending on k , interblade phase angle β , gap to chord ratio s/c , and stagger angle ξ . The total force f_j , in units of pounds, acting on the j^{th} blade, can be expressed as,

$$f_j = \pi \rho \omega^2 b^2 l l_h w_0 e^{i(\omega t + \beta j)} \quad (43)$$

where l is an average span of the blade, and

$$l_h = l_{hR} + i l_{hI} = \frac{2i C_{Fq}}{k} \quad (44)$$

is a nondimensional complex coefficient expressing the lift on the blade due to translation w_0 of the blade at the 3/4 span reference location. Comparing the above expression for f_j with the general f_j given in Eq. (3), one notes that the aerodynamic coefficients A_R and A_I for this problem are,

$$\begin{aligned} A_R &= \pi \rho \omega^2 b^2 l l_{hR} \\ A_I &= \pi \rho \omega^2 b^2 l l_{hI} \end{aligned} \quad (45)$$

The basic equations of motion for bending vibrations of the blades Eq. (1), can be rewritten in the alternate form,

$$m \ddot{w}_j + \underbrace{2 \zeta_s \omega_n m \dot{w}_j}_{\text{"c"}} + \underbrace{m \omega_n^2 w_j}_{\text{"k"}} = f_j \quad (46)$$

$j = 1, 2, \dots, N$

where ω_n is the natural frequency of a blade, and ζ_s is the critical damping ratio of the structural vibrations. With these definitions, and using the relations for A_R and A_I given by Eqs. (45), the criterion for instability of Eq. (4d) becomes,

$$\omega \, 2 \zeta_s \omega_n m - \pi \rho \omega^2 b^2 l l_{hI} < 0 \quad (47)$$

Recognizing from the real equation, Eq. (4a) that approximately $\omega \approx \omega_n$, the above criterion reduces to

$$\zeta_s + \zeta_A < 0 \quad (48)$$

where one defines the important nondimensional quantities as,

$$\begin{aligned} \zeta_A &\equiv -\frac{l_{hI}}{2\mu} && \text{aerodynamic damping ratio} \\ \mu &\equiv \frac{m}{\pi \rho b^2 l} && \text{mass density ratio} \end{aligned} \quad (49)$$

For instability, it is seen from Eq. (48) that the aerodynamic damping ζ_A must be negative. This implies that l_{hI} must be positive. Also, it is to be noted from Eqs. (49), that for heavy blades (μ large), the aerodynamic damping becomes less effective than the inherent structural damping ζ_s .

Values of l_h and ζ_A using Whitehead's theory (Ref. 4) are shown in Table I and Fig. 5. The aerodynamic damping is plotted against increasing reduced velocity $V/\omega b$ for several interblade phase angles β and stagger angles $\xi = 0$ and 45° . Since ζ_A is always positive, pure bending flutter cannot occur, according to 2-dimensional incompressible, cascade theory.

Table 2 shows values of l_h according to Theodorsen's 2-dimensional incompressible, single airfoil theory, Ref. 5. The values resemble somewhat the $\beta = 90^\circ$ values for the zero stagger cascade analysis. Again, pure bending flutter cannot occur.

7. Application to Torsion Flutter

The pure torsion flutter of a rotor disk will also be examined using the simpler traveling wave theory described in Section 2. The geometrical layout of the rotor stage is shown in Fig. 6. It is assumed that the blades have thin, symmetric sections which can pivot around the midchord. Again, Whitehead's 2-dimensional, incompressible cascade theory in Ref. 4 will be used.

The aerodynamic moment per unit span about the elastic axis, acting on the j^{th} blade of a cascade is given by Whitehead as,

$$\begin{aligned}\bar{M}_j &= \pi \rho V^2 c^2 \alpha_o (C_{M\alpha})_\eta e^{i(\omega t + \beta j)} \\ &= \pi \rho \omega^2 b^4 \left[\frac{4}{k^2} (C_{M\alpha})_\eta \right] \alpha_o e^{i(\omega t + \beta j)}\end{aligned}\quad (50)$$

where b = semichord, $k = \omega b/V$ is the reduced frequency, and $(C_{M\alpha})_\eta$ is a nondimensional complex coefficient depending on elastic axis location η , reduced frequency k , interblade phase angle β , gap to chord ratio s/c , and stagger angle ξ . The total moment \bar{m}_j , in units of foot-pounds acting on the j^{th} blade, can be expressed as,

$$\bar{m}_j = \pi \rho \omega^2 b^4 \ell m_\alpha \alpha_o e^{i(\omega t + \beta j)}\quad (51)$$

where ℓ is in an average span of the blade, and

$$\begin{aligned}
 m_\alpha &= m_{\alpha R} + i m_{\alpha I} \\
 &= \frac{4}{b^2} \left[C_{M\alpha} - \eta C'_{F\alpha} - i 2k\eta C'_{Mq} + i 2k\eta^2 C'_{Fq} \right] \quad (52)
 \end{aligned}$$

is a nondimensional complex coefficient expressing the moment about the elastic axis location η . For this work, the elastic axis location is taken at the midchord $\eta = .5$, and the remaining coefficients $C_{M\alpha}$, $C_{F\alpha}$, C_{Mq} , and C_{Fq} are tabulated in Ref. 4. Comparing the above expression for \bar{m}_j with the general expression in the form of Eq. (3) namely,

$$\bar{m}_j = (A_R + i A_I) \alpha_0 e^{i(\omega t + \beta j)} \quad (53)$$

gives the aerodynamic coefficients A_R and A_I for this problem as,

$$\begin{aligned}
 A_R &= \pi \rho \omega^2 b^4 l m_{\alpha R} \\
 A_I &= \pi \rho \omega^2 b^4 l m_{\alpha I}
 \end{aligned} \quad (54)$$

The basic equations of motion for pure torsional vibrations of the blades corresponding to Eq. (1) are,

$$I \ddot{\alpha}_j + c \dot{\alpha}_j + k \alpha_j = \bar{m}_j \quad (55)$$

$j = 1, 2, \dots, N$

or alternatively, these can be rewritten as,

$$I \ddot{\alpha}_j + \underbrace{2 \zeta_s \omega_n I}_{\text{"c"}} \dot{\alpha}_j + \underbrace{I \omega_n^2}_{\text{"h"}} \alpha_j = \bar{m}_j \quad (56)$$

$j = 1, 2, \dots, N$

where ω_n is the torsional natural frequency of a blade, and ζ_s is the critical damping ratio of the structural vibrations. Using these new definitions for torsion, and following through as in the previous bending case in Section 6, the criterion for instability of Eq. (4d) reduces again to,

$$\zeta_s + \zeta_A < 0 \quad (48)$$

where one now defines the important nondimensional quantities as

$$\begin{aligned} \zeta_A &\equiv - \frac{m_{\alpha I}}{2 \mu r_\alpha^2} && \text{aerodynamic damping ratio} \\ \mu &\equiv \frac{m}{\pi \rho b^2 l} && \text{mass density ratio} \\ r_\alpha &\equiv \sqrt{\frac{I_\alpha}{m b^2}} && \text{radius of gyration ratio} \end{aligned} \quad (57)$$

Again, for instability, it is seen from Eq. (48) that the aerodynamic damping ζ_A must be negative, which implies that $m_{\alpha I}$ must be positive. Also, it is again noted that for heavy blades (μr_α^2 large), the aerodynamic damping becomes less effective than the inherent structural damping ζ_s .

Values of m_α and ζ_A using Whitehead's theory (Ref. 4) are shown in Table 3 and Fig. 7 for the elastic axis at midchord ($\eta = .5$). The aerodynamic damping is again plotted against increasing reduced velocity V/wb for several interblade phase angles β and stagger angles $\xi = 0^\circ$ and 45° . It is seen a flutter instability condition can occur for the staggered cascade $\xi = 45^\circ$ with interblade phase angles $\beta \approx 90^\circ$ above reduced velocities $V/wb \approx 3$. However, no flutter occurs for the unstaggered $\xi = 0^\circ$ cascade.

Table 4 shows values of m_α according to Theodorsen's 2-dimensional, incompressible, single airfoil theory, Ref. 5. The values resemble somewhat the $\beta = 90^\circ$ values for the zero stagger cascade analysis. No torsional flutter instability occurs for these blades according to this theory.

8. Combined Bending-Torsion Flutter

In addition to the pure bending and pure torsion flutter considered in the previous two sections, there is always the possibility, as in aircraft wing flutter, of a coupled bending-torsion flutter of the blades. This may arise if the center of gravity of the section does not lie on the elastic axis, or through aerodynamic coupling between the modes. Additionally, there may be structural coupling between bending and torsion through flexible disk and shroud motions. Such structural couplings will be considered in Part B. The bending-torsion analysis here will be limited to thin blades without shrouds, mounted on comparatively rigid disks.

The equations of motion for bending-torsion flutter can be represented by $N = 23$ identical pairs of blade equations of the form,

$$\begin{aligned} m \ddot{w}_j + S \ddot{\alpha}_j + c_w \dot{w}_j + k_w w_j &= f_j \\ S \ddot{w}_j + I \ddot{\alpha}_j + c_\alpha \dot{\alpha}_j + k_\alpha \alpha_j &= \bar{m}_j \end{aligned} \quad (58)$$

$j = 1, 2, \dots, N$

where S represents the static unbalance about the elastic axis and the remaining quantities have been defined previously for the pure bending and pure torsion cases. The w_j and α_j now represent the bending and torsion motions of the elastic axis, and are separate degrees of freedom here. Because the blades are mounted on a circular ring, one again looks for traveling wave solutions of the form,

$$\begin{aligned} w_j &= w_0 e^{i(\omega t + \beta j)} \\ \alpha_j &= \alpha_0 e^{i(\omega t + \beta j)} \end{aligned} \quad (59)$$

where w_0 and α_0 may be complex quantities. Note: To obtain the physical significance of the above vibrations, one takes the real part as in Eq. (2a), only now since w_0 and α_0 may be complex, additional phasings between the w_j and α_j vibrations are possible.

The airforces corresponding to the motions of Eqs. (59) about the elastic axis location η , have been given by Whitehead in Ref. 4 as,

$$\begin{aligned}
F_j &= \pi \rho V c \left[(C_{Fq})_\eta i \omega W_o - (C_{Fa})_\eta V \alpha_o \right] e^{i(\omega t + \beta j)} \\
\bar{M}_j &= \pi \rho V c^2 \left[-(C_{Mq})_\eta i \omega W_o + (C_{Ma})_\eta V \alpha_o \right] e^{i(\omega t + \beta j)} \quad (60)
\end{aligned}$$

These represent the forces per unit span, acting on the j^{th} blade of a cascade for 2-Dimensional, incompressible flow. The total forces and moments, in units of pounds and foot-pounds respectively, can be expressed as

$$\begin{aligned}
f_j &= \pi \rho \omega^2 b^3 l \left[l_h \frac{W_o}{b} + l_\alpha \alpha_o \right] e^{i(\omega t + \beta j)} \\
\bar{m}_j &= \pi \rho \omega^2 b^4 l \left[m_h \frac{W_o}{b} + m_\alpha \alpha_o \right] e^{i(\omega t + \beta j)} \quad (61)
\end{aligned}$$

where l is an average span of the blade and $l_h, l_\alpha, m_h, m_\alpha$ are nondimensional complex coefficients which can be related to the tabulated Whitehead coefficients by comparing Eqs. (60) and (61). In fact, these relations are,

$$\begin{aligned}
l_h &= \frac{2i}{k} C_{Fq} \\
l_\alpha &= \frac{2}{k^2} \left[-C_{Fa} + i 2 k \eta C_{Fq} \right] \\
m_h &= \frac{4i}{k} \left[-C_{Mq} + \eta C_{Fq} \right] \\
m_\alpha &= \frac{4}{k^2} \left[C_{Ma} - \eta C_{Fa} - i 2 k \eta C_{Mq} + i 2 k \eta^2 C_{Fq} \right] \quad (62)
\end{aligned}$$

where η defines the location of the elastic axis.

Placing the assumed solutions Eqs. (59) and the corresponding airforces Eqs. (61) into the equations of motion, Eqs. (58), results in two complex homogeneous equations in w_0 and α_0 . For non-trivial solutions of w_0 and α_0 , one seeks appropriate values that make the resulting complex determinant equal to zero (both real part and imaginary part, simultaneously). This then represents the flutter traveling wave solution given by Eq. (59).

Coupled bending-torsion solutions of the type described above, were carried out extensively by Friedmann and Bendiksen in Ref. 6. These used Whitehead's 2-Dimensional, incompressible cascade theory, and required considerable numerical computation to match the required conditions and to arrive at the minimum flutter speed, for a given configuration. Some typical results from Ref. 6 are given in Fig. 8 showing the effects of static unbalance on the flutter speed. Considerable reduction below the pure torsion flutter case is possible for some configurations.

The coupled bending-torsion flutter described in this section can be characterized as a "Two Degree of Freedom, Traveling Wave Flutter". The phase angle ϕ between the bending and torsion motion in Eqs. (59), plays an important role in allowing flutter to exist. This structural coupling angle ϕ is free to be determined here from the two mode analysis, and often turns out to be in the neighborhood of 90° . The structural coupling angle ϕ between the bending and torsion motions, should not be confused with the interblade phase angle β , which remains a separate parameter in these equations. This kind of two mode analysis is applicable for thin blades, without shrouds, mounted on comparatively rigid disks.

It should be mentioned that the use of Theodorsen's 2-dimensional, incompressible, single airfoil theory, Ref. 5, will lead to flutter instability for these coupled bending-torsion cases. This is in contrast to the pure bending and pure torsion case where flutter does not occur. Also, it should be remarked that a limited number of such two degree of freedom analyses were claimed to have been performed by Whitehead in Ref. 4, and found to have little effect on the single degree of freedom calculations. The work of Friedmann and Bendiksen, Ref. 6, seems to have explored these two degree of freedom solutions on a much larger scale, and over a wider range of parameters.

PART B: FLEXIBLE DISK

Assume a balanced, tuned rotor with a flexible disk. The blades also may have shrouds connecting them. Structural coupling as well as aerodynamic coupling exists between the blades. See Fig. 9. The vibration modes of the overall blade-disk system will first be described, in terms of both standing waves and traveling waves. Then, a traveling wave flutter analysis will be performed.

9. Description of Vibration Modes

For the flexible, interconnected blade-disk assembly, one can obtain the overall vibration, modes by a finite element analysis. There will generally be two standing wave vibration modes q_1 and q_2 for a given nodal diameter n , which corresponds to $\sin n\theta$ and $\cos n\theta$ disk modes. The basic equations for a given nodal diameter n can be written as,

$$\begin{aligned} M \ddot{q}_1 + C \dot{q}_1 + K q_1 &= Q_1 \\ M \ddot{q}_2 + C \dot{q}_2 + K q_2 &= Q_2 \end{aligned} \tag{63}$$

For the 1st mode q_1 above, the deflection and angle at any blade j is,

$$\begin{aligned} w_j &= (b h_o \cos \beta j) q_1 \\ \alpha_j &= (\alpha_c \cos \beta j + \alpha_s \sin \beta j) q_1 \end{aligned} \tag{64}$$

where b = semichord of reference station, and h_0 , α_c , α_s are nondimensional quantities that are found from the overall vibration modes of the disk assembly. See Fig. 10. The overall M , C , K corresponding to this mode can also be evaluated from the standing wave, finite element vibration analysis. It is to be noted from Eq. (64) that q_1 and q_2 here are nondimensional coordinates.

In the above representation, the α_c and α_s give how much the angle at the blade changes for a given blade deflection, bh_0 . For example, for a flexible rotor with blades having their C.G. coincide with the blade elastic axis, a flexible disk deflection of the n^{th} circumferential mode $w_D \cos n\theta$, would cause a blade deflection and twist of the form,

$$\begin{aligned} W &= (w_D \sin \xi + w_B) \cos \beta j \\ \alpha &= \left(-\frac{w_D}{R} n + \alpha_B \right) \sin \beta j \end{aligned} \quad (65)$$

In the above, w_D is the disk deflection at the base of the blade, and w_B and α_B are additional flexible blade deflections which are excited by the disk deflection. See Fig. 11. Hence, the h_0 , α_c , α_s for this case are,

$$\begin{aligned} h_0 &= \frac{w_D}{b} \sin \xi + \frac{w_B}{b} \\ \alpha_c &= 0 \\ \alpha_s &= -\frac{w_D}{R} n + \alpha_B \end{aligned} \quad (66)$$

If the blade C.G. does not lie on the blade elastic axis, the inertia unbalance $S\ddot{w}_j$ will cause additional twists α proportional to $w_D \cos n\theta$, that is, additional terms of the type, $\alpha = c_1 w_D \cos \beta j$, where c_1 is some constant. Thus, α_c would then also be present in Eqs. (66). Similar relations for h_0 , α_c , α_s can be obtained when shrouds are present between the blades. In general, the coefficients h_0 , α_c , α_s are obtained from a vibration analysis of the rotor blade-disk assembly (usually by the finite element method).

As mentioned earlier, 2 modes are present for each frequency ω_n corresponding roughly to the two disk modes $\sin n\theta$ and $\cos n\theta$. Because of symmetry relations, the second mode q_2 nodal pattern is related to the first mode q_1 , by a phase shift of 90° . See Fig. 12. Thus, for the 2nd mode q_2 , one has,

$$\begin{aligned} w_j &= [bh_0 \cos(\beta j - 90^\circ)] q_2 = [bh_0 \sin \beta j] q_2 \\ \alpha_j &= [\alpha_c \cos(\beta j - 90^\circ) + \alpha_s \sin(\beta j - 90^\circ)] q_2 \quad (67) \\ &= [\alpha_c \sin \beta j - \alpha_s \cos \beta j] q_2 \end{aligned}$$

Hence, in the basic modal Eqs. (63), the deflections and angles for any blade j are,

$$\begin{aligned} w_j &= (bh_0 \cos \beta j) q_1 + (bh_0 \sin \beta j) q_2 \\ \alpha_j &= (\alpha_c \cos \beta j + \alpha_s \sin \beta j) q_1 \quad (68) \\ &\quad + (\alpha_c \sin \beta j - \alpha_s \cos \beta j) q_2 \end{aligned}$$

The corresponding generalized forces Q_1 and Q_2 for Eqs. (63) can be obtained by considering the incremental work done δW , by the aerodynamic forces over all the blades,

$$\begin{aligned}
 \delta W &= \sum_{j=1}^{23} [f_j \delta w_j + \bar{m}_j \delta \alpha_j] \\
 &= \sum_{j=1}^{23} [f_j (b h_o \cos \beta_j \delta q_1 + b h_o \sin \beta_j \delta q_2) \\
 &\quad + \bar{m}_j (\alpha_c \cos \beta_j + \alpha_s \sin \beta_j) \delta q_1 \\
 &\quad + \bar{m}_j (\alpha_c \sin \beta_j - \alpha_s \cos \beta_j) \delta q_2] = \sum_{i=1}^2 Q_i \delta q_i
 \end{aligned} \tag{69}$$

Hence, in Eqs. (63), the generalized forces are

$$\begin{aligned}
 Q_1 &= \sum_{j=1}^{23} (f_j b h_o \cos \beta_j + \bar{m}_j \alpha_c \cos \beta_j + \bar{m}_j \alpha_s \sin \beta_j) \\
 Q_2 &= \sum_{j=1}^{23} (f_j b h_o \sin \beta_j + \bar{m}_j \alpha_c \sin \beta_j - \bar{m}_j \alpha_s \cos \beta_j)
 \end{aligned} \tag{70}$$

where f_j and \bar{m}_j are the forces and moments about the elastic axis.

Using Eqs. (63), (68), and (70), one can obtain the transient response of a particular nodal diameter disk mode to any aerodynamic forces f_j and \bar{m}_j over the blades. These equations are comparable to Eqs. (8) and (6)

developed earlier in Section 3. They are useful in this form to examine the response to forcing excitation, as mentioned earlier at the end of Section 5.

For the flutter analysis that will be presented in the next section, the simpler traveling wave analysis will be used instead of the above standing wave modal analysis.

10. Traveling Wave Analysis

The basic equations for vibrations in the n^{th} nodal diameter mode were given previously by Eqs. (63), (70) and (68) as,

$$\begin{aligned} M \ddot{q}_1 + C \dot{q}_1 + K q_1 &= \sum_{j=1}^{23} \left(f_j b h_0 \cos \beta_j + \bar{m}_j \alpha_c \cos \beta_j \right. \\ &\quad \left. + \bar{m}_j \alpha_s \sin \beta_j \right) \\ M \ddot{q}_2 + C \dot{q}_2 + K q_2 &= \sum_{j=1}^{23} \left(f_j b h_0 \sin \beta_j + \bar{m}_j \alpha_c \sin \beta_j \right. \\ &\quad \left. - \bar{m}_j \alpha_s \cos \beta_j \right) \end{aligned} \quad (71)$$

where,

$$\begin{aligned} w_j &= (b h_0 \cos \beta_j) q_1 + (b h_0 \sin \beta_j) q_2 \\ \alpha_j &= (\alpha_c \cos \beta_j + \alpha_s \sin \beta_j) q_1 + (\alpha_c \sin \beta_j - \alpha_s \cos \beta_j) q_2 \end{aligned} \quad (68)$$

To obtain traveling wave solutions, multiply the first Eq. (71) by $b h_0 \cos \beta_k$, multiply the second Eq. (71) by $b h_0 \sin \beta_k$, then add to give, as in Section 3.

$$\begin{aligned}
M \ddot{w}_k + C \dot{w}_k + K w_k &= \\
&= b h_0 \cos \beta k \sum_{j=1}^{23} (f_j b h_0 \cos \beta j + \bar{m}_j \alpha_c \cos \beta j + \bar{m}_j \alpha_s \sin \beta j) \\
&\quad + b h_0 \sin \beta k \sum_{j=1}^{23} (f_j b h_0 \sin \beta j + \bar{m}_j \alpha_c \sin \beta j - \bar{m}_j \alpha_s \cos \beta j)
\end{aligned} \tag{72}$$

Recall from Section 5 that traveling wave solutions of the above can be obtained from the standing wave Eqs. (68) by setting

$$\begin{aligned}
q_1 &= q_0 e^{i\omega t} \\
q_2 &= i q_0 e^{i\omega t}
\end{aligned} \tag{73}$$

This would result in,

$$\begin{aligned}
w_k &= b h_0 \cos \beta k q_0 e^{i\omega t} + i b h_0 \sin \beta k q_0 e^{i\omega t} \\
&= b h_0 q_0 e^{i(\omega t + \beta k)}
\end{aligned} \tag{74}$$

The associated twist angle α_k could also be put in a similar form by first setting,

$$\begin{aligned}
\alpha_c &= \alpha_0 \cos \phi \\
\alpha_s &= \alpha_0 \sin \phi
\end{aligned} \tag{75}$$

This would then result in

$$\begin{aligned}
\alpha_k &= (\alpha_0 \cos \phi \cos \beta k + \alpha_0 \sin \phi \sin \beta k) q_0 e^{i\omega t} \\
&\quad + i (\alpha_0 \cos \phi \sin \beta k - \alpha_0 \sin \phi \cos \beta k) q_0 e^{i\omega t} \\
&= \alpha_0 q_0 e^{i(\omega t + \beta k - \phi)}
\end{aligned} \tag{76}$$

where one has defined from Eqs. (75),

$$\alpha_o = \sqrt{\alpha_c^2 + \alpha_s^2}, \quad \phi = \tan^{-1} \frac{\alpha_s}{\alpha_c} \quad (77)$$

Note that in obtaining ϕ from Eqs. (77), one would have more specifically,

$$\begin{array}{llll} \text{If} & \alpha_c = +, \alpha_s = +, & \text{then} & \phi = 0 \text{ to } 90^\circ \\ & \alpha_c = -, \alpha_s = +, & & \phi = 90^\circ \text{ to } 180^\circ \\ & \alpha_c = +, \alpha_s = -, & & \phi = 0 \text{ to } -90^\circ \\ & \alpha_c = -, \alpha_s = -, & & \phi = -90^\circ \text{ to } -180^\circ \end{array} \quad (77a)$$

Corresponding to the traveling wave deflections Eqs. (74) and (76), are the traveling wave airforces given generally in Section 8 by Eqs. (61) as,

$$\begin{aligned} f_j &= \pi \rho \omega^2 b^3 l \left(l_h \frac{\bar{w}}{b} + l_a \bar{\alpha} \right) e^{i(\omega t + \beta j)} \\ \bar{m}_j &= \pi \rho \omega^2 b^4 l \left(m_h \frac{\bar{w}}{b} + m_a \bar{\alpha} \right) e^{i(\omega t + \beta j)} \end{aligned} \quad (61)$$

For the deflection shapes Eqs. (74) and (76), one has,

$$\begin{aligned} \bar{w} &= b h_o q_o \\ \bar{\alpha} &= \alpha_o q_o e^{-i\phi} = \alpha_o q_o (\cos \phi - i \sin \phi) \end{aligned} \quad (78)$$

Placing these into Eqs. (61) gives the corresponding traveling wave airforces as,

$$\begin{aligned} f_j &= \pi \rho \omega^2 b^3 l \left[l_h h_o + l_\alpha e^{-i\phi} \alpha_o \right] q_o e^{i(\omega t + \beta k)} \\ \bar{m}_j &= \pi \rho \omega^2 b^4 l \left[m_h h_o + m_\alpha e^{-i\phi} \alpha_o \right] q_o e^{i(\omega t + \beta k)} \end{aligned} \quad (79)$$

With these airforces, the right-hand-side of Eq. (72) becomes

$$\begin{aligned} \text{R.H.S.} &= \pi \rho \omega^2 b^3 l b h_o \left\{ \cos \beta k \sum_{j=1}^{23} \left[l_h h_o + l_\alpha e^{-i\phi} \alpha_o \right] b h_o \cos \beta j \right. \\ &\quad + \cos \beta k \sum_{j=1}^{23} b \left[m_h h_o + m_\alpha e^{-i\phi} \alpha_o \right] \alpha_o \cos \phi \cos \beta j \\ &\quad + \cos \beta k \sum_{j=1}^{23} b \left[m_h h_o + m_\alpha e^{-i\phi} \alpha_o \right] \alpha_o \sin \phi \sin \beta j \\ &\quad + \sin \beta k \sum_{j=1}^{23} \left[l_h h_o + l_\alpha e^{-i\phi} \alpha_o \right] b h_o \sin \beta j \\ &\quad + \sin \beta k \sum_{j=1}^{23} b \left[m_h h_o + m_\alpha e^{-i\phi} \alpha_o \right] \alpha_o \cos \phi \sin \beta j \\ &\quad \left. - \sin \beta k \sum_{j=1}^{23} b \left[m_h h_o + m_\alpha e^{-i\phi} \alpha_o \right] \alpha_o \sin \phi \cos \beta j \right\} \\ &\quad \times (\cos \beta j + i \sin \beta j) q_o e^{i\omega t} \end{aligned} \quad (80)$$

Introducing the previous trigonometric relations Eqs. (7) for the summations over j , that is,

$$\begin{aligned} \sum_{j=1}^{23} \cos^2 \beta j &= \sum_{j=1}^{23} \sin^2 \beta j = \frac{N}{2} \\ \sum_{j=1}^{23} \sin \beta j \cos \beta j &= 0 \end{aligned} \quad (7)$$

The R.H.S. of Eq. (80) becomes,

$$\begin{aligned}
 \text{R.H.S.} = & \pi \rho \omega^2 b^4 l b h_0 q_0 e^{i\omega t} \times \\
 & \times \left\{ \cos \beta k \left[l_h h_0 + l_\alpha e^{-i\phi} \alpha_0 \right] h_0 \frac{N}{2} \right. \\
 & + \cos \beta k \left[m_h h_0 + m_\alpha e^{-i\phi} \alpha_0 \right] \alpha_0 \cos \phi \frac{N}{2} \\
 & + \cos \beta k \left[m_h h_0 + m_\alpha e^{-i\phi} \alpha_0 \right] \alpha_0 \sin \phi i \frac{N}{2} \\
 & + \sin \beta k \left[l_h h_0 + l_\alpha e^{-i\phi} \alpha_0 \right] h_0 i \frac{N}{2} \\
 & + \sin \beta k \left[m_h h_0 + m_\alpha e^{-i\phi} \alpha_0 \right] \alpha_0 \cos \phi i \frac{N}{2} \quad (81) \\
 & \left. - \sin \beta k \left[m_h h_0 + m_\alpha e^{-i\phi} \alpha_0 \right] \alpha_0 \sin \phi \frac{N}{2} \right\}
 \end{aligned}$$

$$\begin{aligned}
 \text{R.H.S.} = & \pi \rho \omega^2 b^4 l \frac{N}{2} b h_0 q_0 e^{i\omega t} \times \\
 & \times \left\{ e^{i\beta k} \left[l_h h_0 + l_\alpha e^{-i\phi} \alpha_0 \right] h_0 \right. \\
 & + e^{i\beta k} \left[m_h h_0 + m_\alpha e^{-i\phi} \alpha_0 \right] \alpha_0 \cos \phi \\
 & \left. + e^{i\beta k} i \left[m_h h_0 + m_\alpha e^{-i\phi} \alpha_0 \right] \alpha_0 \sin \phi \right\}
 \end{aligned}$$

which eventually reduces to,

$$\begin{aligned} \text{R.H.S.} &= \pi \rho \omega^2 b^4 l \frac{N}{2} b h_0 q_0 e^{i(\omega t + \beta h)} \times \\ &\times \left\{ l_h h_0^2 + [l_\alpha e^{-i\phi} + m_h e^{+i\phi}] h_0 \alpha_0 + m_\alpha \alpha_0^2 \right\} \end{aligned} \quad (82)$$

Now, placing Eq. (82) together with the traveling wave deflection Eq. (74) back into Eq. (72) gives,

$$\begin{aligned} -\omega^2 M \cancel{b h_0 q_0 e^{i(\omega t + \beta h)}} + i\omega C \cancel{b h_0 q_0 e^{i(\omega t + \beta h)}} + K \cancel{b h_0 q_0 e^{i(\omega t + \beta h)}} &= \\ = \pi \rho \omega^2 b^4 l \frac{N}{2} \cancel{b h_0 q_0 e^{i(\omega t + \beta h)}} \bar{A} \end{aligned} \quad (83)$$

where \bar{A} is a nondimensional, complex aerodynamic coefficient defined by,

$$\bar{A} \equiv l_h h_0^2 + [l_\alpha e^{-i\phi} + m_h e^{+i\phi}] h_0 \alpha_0 + m_\alpha \alpha_0^2 \quad (84)$$

Equation (83) reduces to the familiar real and imaginary equations as in Eqs. (12) and (4),

$$\text{Real Eq.:} \quad -\omega^2 M + K - \frac{N}{2} \pi \rho \omega^2 b^4 l \bar{A}_R = 0 \quad (85)$$

$$\text{Imag. Eq.:} \quad \omega C - \frac{N}{2} \pi \rho \omega^2 b^4 l \bar{A}_I = 0$$

Further defining C and K as in Eq. (46) and introducing the mass density ratio μ , namely,

$$\begin{aligned}
 C &= 2 \zeta_s \omega_n M \\
 K &= M \omega_n^2 \\
 \mu &= \frac{M}{\pi \rho b^2 l N/2}
 \end{aligned}
 \tag{86}$$

the real equation of Eq. (85) reduces simply to,

$$\omega^2 = \omega_n^2 \left(1 - \frac{\bar{A}_R}{\mu} \right) \tag{87}$$

As mentioned in Section 2, usually $\bar{A}_R/\mu \ll 1$ for these rotor disks and hence approximately $\omega \approx \omega_n$. The imaginary equation of Eq. (85) then reduces to the simple criterion for instability,

$$\zeta_s + \zeta_A < 0 \tag{48}$$

where one defines the important nondimensional aerodynamic damping,

$$\zeta_A \equiv - \frac{\bar{A}_I}{2\mu} \tag{88}$$

and \bar{A}_I is the imaginary part of the nondimensional function \bar{A} given by Eq. (84). For instability, it is seen from Eq. (48) that the aerodynamic damping ζ_A must be negative. This implies \bar{A}_I must be positive.

The important part of the aerodynamic coefficient \bar{A} for flutter considerations is the imaginary part. This can be worked out from the general expression for \bar{A} in Eq. (84) to give,

$$\bar{A}_I = l_{hI} h_o^2 + \left[(l_{\alpha I} + m_{hI}) \cos \phi + (-l_{\alpha R} + m_{hR}) \sin \phi \right] h_o \alpha_o + m_{\alpha I} \alpha_o^2 \tag{89}$$

This agrees with the expression given by Carta in Ref. 2 except for some sign differences due to different assumed directions for some of the forces and deflections. Also, this expression together with Eq. (88) reduces to the pure bending and pure torsion criteria given previously in Eqs. (49) and (57). It should be mentioned, that often the h_0 , α_c , α_s coefficients in Eqs. (64) are picked such that $h_0 = 1$. Then α_c and α_s represent the amount of twist present for a unit h_0 blade deflection. See Eq. (64).

The type of flutter described in this section for flexible disks can be characterized as "Single Degree of Freedom, Travleing Wave Flutter", since it involves a single unknown coordinate q_0 . The critical nondimensional coefficient \bar{A}_I is a function of reduced frequency $\omega b/V$, gap to chord ratio s/c , stagger angle ξ , interblade phase angle β , and structural coupling angle ϕ . The latter two angles should not be confused. The interblade phase angle β comes from aerodynamic coupling between the blades, while the structural coupling angle ϕ comes from the mechanical coupling between blades. Because of the structural coupling angle ϕ , the \bar{A}_I coefficient can become positive even without the aerodynamic coupling between the blades. One can obtain flutter with single blade aerodynamics such as Theodorsen's theory in Ref. 5 if ϕ is near an angle of about 90° . This type of flutter due to ϕ alone and $\beta = 0$, is a standing wave type flutter.

The presence of this structural coupling angle ϕ is what mainly causes the type of blade-disk-shroud flutter originally described by F. Carta in Ref. 2. In general however, aerodynamic coupling β will also be present

in addition to the structural coupling ϕ . The value of β that makes the $\zeta_S + \zeta_A$ most negative is the flutter that would occur first. Generally this would be for $\beta \neq 0$ or $\beta \neq 180^\circ$, hence it would be a traveling wave type flutter.

II. Further Remarks on Flutter

The flutter analysis for the flexible disk rotors considered in the previous section, was essentially a single degree of freedom analysis involving the single coordinate q_0 . In there, the flutter mode is assumed to be identical to the vacuum vibration mode, thus fixing the structural coupling angle ϕ between the bending and torsion motions to that obtained from the vacuum vibration mode analysis. However, as was seen in Section 8, it is conceivable that under some conditions, this angle ϕ may be changed by the flutter phenomenon. To allow for this possibility, one should perform two degree of freedom, traveling wave analyses as was done in Section 8.

To perform such a two degree of freedom analysis, one would pick two pairs of standing wave vibration modes for the n^{th} nodal diameter, each pair consisting of a $\sin n\theta$ and $\cos n\theta$ disk mode. One pair would be picked with a large blade bending contribution and the other pair with a large blade torsion contribution. Following Eq. (68), the deflections would be,

$$\begin{aligned}
w_j &= (b h_0 \cos \beta_j) q_1 + (b h_0 \sin \beta_j) q_2 \\
&\quad + (b \tilde{h}_0 \cos \beta_j) \tilde{q}_1 + (b h_0 \sin \beta_j) \tilde{q}_2 \\
\alpha_j &= (\alpha_c \cos \beta_j + \alpha_s \sin \beta_j) q_1 + (\alpha_c \sin \beta_j - \alpha_s \cos \beta_j) q_2 \\
&\quad + (\tilde{\alpha}_c \cos \beta_j + \tilde{\alpha}_s \sin \beta_j) \tilde{q}_1 + (\tilde{\alpha}_c \sin \beta_j - \tilde{\alpha}_s \cos \beta_j) \tilde{q}_2
\end{aligned} \tag{90}$$

where \tilde{q}_1 , \tilde{q}_2 , \tilde{h}_0 , $\tilde{\alpha}_c$, $\tilde{\alpha}_s$ are values associated with the second pair of modes. The corresponding equations of motion following Eqs. (71) would then be

$$\begin{aligned}
M \ddot{q}_1 + C \dot{q}_1 + K q_1 &= \sum_j (f_j b h_0 \cos \beta_j + \dots) \\
M \ddot{q}_2 + C \dot{q}_2 + K q_2 &= \sum_j (f_j b h_0 \sin \beta_j + \dots) \\
\tilde{M} \ddot{\tilde{q}}_1 + \tilde{C} \dot{\tilde{q}}_1 + \tilde{K} \tilde{q}_1 &= \sum_j (f_j b \tilde{h}_0 \cos \beta_j + \dots) \\
\tilde{M} \ddot{\tilde{q}}_2 + \tilde{C} \dot{\tilde{q}}_2 + \tilde{K} \tilde{q}_2 &= \sum_j (f_j b \tilde{h}_0 \sin \beta_j + \dots)
\end{aligned} \tag{91}$$

Traveling wave solutions of these equations can be obtained from the standing wave deflections Eqs. (90) by setting,

$$\begin{aligned}
q_1 &= q_0 e^{i\omega t} & \tilde{q}_1 &= \tilde{q}_0 e^{i\omega t} \\
q_2 &= i q_0 e^{i\omega t} & \tilde{q}_2 &= i \tilde{q}_0 e^{i\omega t}
\end{aligned} \tag{92}$$

This would result in blade deflections,

$$W_k = b h_0 q_0 e^{i(\omega t + \beta k)} + b \tilde{h}_0 \tilde{q}_0 e^{i(\omega t + \beta k)} \quad (93)$$

and similarly for α_k . Then following through as in Section 10, one can reduce the four equations of Eqs. (91) to two equations of the form,

$$\begin{aligned} & \left[-\omega^2 M + i\omega C + K \right] b h_0 q_0 e^{i(\omega t + \beta k)} = \\ & = b h_0 \cos \beta k \sum_j^j (f_j b h_0 \cos \beta j + \dots) + b h_0 \sin \beta k \sum_j^j (f_j b h_0 \sin \beta j + \dots) \\ & \left[-\omega^2 \tilde{M} + i\omega \tilde{C} + \tilde{K} \right] b \tilde{h}_0 \tilde{q}_0 e^{i(\omega t + \beta k)} = \\ & = b \tilde{h}_0 \cos \beta k \sum_j^j (f_j b \tilde{h}_0 \cos \beta j + \dots) + b \tilde{h}_0 \sin \beta k \sum_j^j (f_j b \tilde{h}_0 \sin \beta j + \dots) \end{aligned} \quad (94)$$

Equations (94) above represent two simultaneous equations in the two complex unknowns q_0 and \tilde{q}_0 . They are coupled together through the aerodynamic forces f_j and \bar{m}_j on the right-hand-side since these aerodynamic forces depend on w_k and α_k as indicated by Eq. (93). These equations can be analyzed and solved in the manner indicated in Section 8 for the coupled bending - Torsion flutter. Such two degree of freedom, traveling wave flutter analyses for flexible rotors, represent a transition between the

rigid disk rotor case (where the structural coupling angle ϕ is free to be determined by the inertial and aerodynamic coupling, Section 8), and the flexible disk rotor case (where the structural coupling angle ϕ is assumed fixed at the vacuum free vibration mode result, Section 10).

It should be remarked that in the past, it has been customary to assume that because of the large mass density ratio μ of the blades and the strong structural interconnections, the vacuum vibration mode would not change substantially during the flutter condition. Hence the efficacy of the single degree of freedom, traveling wave analyses for blade-disk-shroud flutter given in the previous Section 10, and which were originally described by Carta in Ref. 2. Still, however, there may be situations where a two degree of freedom, traveling wave analysis may be required.

In summary, one can identify several different types of flutter behavior.

A. Flutter of Blades on Rigid Disks - Here, the blades are mounted on comparatively rigid disks, without shrouds. The structural coupling angle from vacuum free vibration modes tends to be $\phi = 0^\circ$ or 180° . Single degree of freedom analyses as in Sections 6 and 7 can show traveling wave flutter ($\beta \neq 0$ or 180°) due to aerodynamic coupling effects between the blades, for staggered blade cases. It is probably good to do two degree of freedom analyses as in Section 8, since these allow the structural coupling angle ϕ to adjust itself to that required by the flutter condition.

- B. Blade-Disk-Shroud Flutter - Here, the blades are mounted on flexible disks, and may have interconnecting shrouds. The structural coupling angle from vacuum free vibration modes tends to be $\phi \approx \pm 90^\circ$. Single degree of freedom analyses as in Section 10 can show standing wave flutter ($\beta = 0$ or 180°) due to the structural coupling angle ϕ even without aerodynamic coupling effects between the blades (Theodorsen's single airfoil theory, Ref. 5). But more likely, it will occur with some aerodynamic coupling effects present, in which case it would appear as a traveling wave type flutter ($\beta \neq 0, 180^\circ$). Two degree of freedom analyses, which allow adjustment of the structural coupling ϕ away from the vacuum vibration modes value, are probably not as important here as for blades on rigid disks.
- C. Stall Flutter - This involves aerodynamic coefficients that are dependent on initial angle and on amplitude of vibration. Single degree of freedom flutter analyses are generally sufficient here, as the phenomenon usually involves a loss of stability of the aerodynamic forces, rather than coupling of modes. Both steady wave or traveling wave flutter may be experienced.

The obtaining of suitable aerodynamic force coefficients for all the different operating regimes of a rotor disk assembly, i.e., subsonic, transonic, supersonic, etc. is a formidable task. In a more complete study, one would try to account for three dimensional flow effects in the rotor. Perhaps computational aerodynamic analyses could be of help here.

Additionally, the flutter behavior of a rotor that is not completely tuned, i.e., some blades are slightly different from others, may also present some interesting local behavior, instead of the uniform traveling wave behavior discussed here. In this connection, the standing wave form of flutter analysis may prove useful.

12. Conclusions

1. The flutter behavior of rotor disk assemblies with both rigid and flexible disks is reviewed in detail.
2. The relations between traveling and standing wave analyses are described in detail, and are shown to be equivalent.
3. The standing wave analyses are shown to be more versatile for some applications, such as the response to forced excitation, than the simpler traveling wave analyses.
4. The separate roles of aerodynamic coupling through interblade phase angle β , and structural coupling through the structural coupling angle ϕ , are described in detail.
5. In addition to the conventional single degree of freedom traveling wave analyses, some two degree of freedom traveling wave analyses are reviewed and described.
6. Extensions to forced vibration problems are indicated.

References

1. Mikolajczak, A. A., Arnoldi, R. A., Snyder, L. E., and Stargardter, H., "Advances in Fan and Compressor Blade Flutter Analysis and Predictions," J. of Aircraft, Vol. 10, No. 4, April 1975, pp. 325-332.
2. Carta, F. O., "Coupled Blade-Disc-Shroud Flutter Instabilities in Turbojet Engine Rotors," ASME Transactions, Journal of Engineering for Power, Vol. 89, July 1967, pp. 419-426.
3. Snyder, L. E., and Commerford, G. L., "Supersonic Unstalled Flutter in Fan Rotor: Analytic and Experimental Results," ASME Paper 74-GT-40, 1974.
4. Whitehead, D. S., "Force and Moment Coefficients for Vibrating Airfoils in Cascade," R. & M. 3254, British Aeronautical Research Council, London, February 1960.
5. Bisplinghoff, R. L., Ashely, H., and Halfman, R. L., Aeroelasticity, Addison-Wesley Publishing Co., Cambridge, Mass., Section 5-6.
6. Friedmann, P., and Bendiksen, O., "Coupled Bending-Torsion Flutter in Cascades," AIAA/ASME/ASCE/AHS 20th Structures, Structural Dynamics and Materials Conference, St. Louis, Mo., April 4-6, 1979.

TABLE 1: VALUES OF ℓ_h FROM WHITEHEAD CASCADE THEORY

$s/c = 1, \quad \xi = 0^\circ$			$s/c = 1, \quad \xi = 45^\circ$		
β	C_{Fq}	ℓ_h	β	C_{Fq}	ℓ_h
<u>$k = 1, (\lambda = 2)$</u>			<u>$k = 1, (\lambda = 2)$</u>		
0°	-.301 -.367 i	.734 -.602 i	0°	-.423 -.455 i	.910 -.846 i
90°	-.587 -.385 i	.770 -1.174 i	90°	-.642 -.386 i	.772 -1.284 i
180°	-.732 -.382 i	.764 -1.464 i	180°	-.680 -.318 i	.636 -1.360 i
270°	-.587 -.385 i	.770 -1.174 i	270°	-.481 -.359 i	.718 -.962 i
<u>$k = .5, (\lambda = 1)$</u>			<u>$k = .5, (\lambda = 1)$</u>		
0°	-.303 -.183 i	.732 -1.21 i	0°	-.426 -.227 i	.908 -1.70 i
90°	-.672 -.037 i	.148 -2.69 i	90°	-.782 -.124 i	.496 -3.13 i
180°	-.876 +.016 i	-.064 -3.50 i	180°	-.846 +.035 i	-.140 -3.38 i
270°	-.672 -.037 i	.148 -2.69 i	270°	-.525 +.022 i	-.088 -2.10 i
<u>$k = .25, (\lambda = .5)$</u>			<u>$k = .25, (\lambda = .5)$</u>		
0°	-.304 -.091 i	.728 -2.43 i	0°	-.427 -.113 i	.904 -3.42 i
90°	-.838 +.136 i	-1.088 -6.70 i	90°	-.930 -.085 i	.680 -7.44 i
180°	-1.096 +.167 i	-1.336 -8.77 i	180°	-1.044 +.132 i	-1.056 -8.35 i
270°	-.838 +.136 i	-1.088 -6.70 i	270°	-.664 +.250 i	-2.00 -5.31 i
<u>$k = .1, (\lambda = .2)$</u>			<u>$k = .1, (\lambda = .2)$</u>		
0°	-.305 +.307 i	-.740 -6.10 i	0°	-.427 -.045 i	.900 -8.45 i
90°	-1.022 +.125 i	-2.50 -20.4 i	90°	-.994 -.173 i	3.46 -19.9 i
180°	-1.270 +.117 i	-2.34 -25.4 i	180°	-1.167 +.081 i	-1.62 -23.3 i
270°	-1.022 +.125 i	-2.50 -20.4 i	270°	-.842 +.313 i	-6.26 -16.8 i

TABLE 2: VALUES OF l_h FROM THEODORSEN SINGLE AIRFOIL THEORY

$$l_h = 1 - i \frac{2 C'(k)}{k}$$

k	C (k)	l_h	$\frac{V}{b\omega}$
1	.539 -.100 i	.800 -1.08 i	1
.5	.598 -.151 i	.396 -2.39 i	2
.25	.693 -.185 i	-.480 -5.54 i	4
.1	.832 -.172 i	-2.44 -16.64 i	10

TABLE 3: VALUES OF m_α FROM WHITEHEAD CASCADE THEORY

$$s/c = 1, \quad \xi = 0^\circ$$

β	$C_{M\alpha}$	$C_{F\alpha}$	C_{Mq}	C_{Fq}	m_α
<u>$k = 1, (\lambda = 2)$</u>					
0°	.1607-.3935 i	.0626 -.8602 i	-.0544-.1854 i	-.3009-.3671 i	.510-.238 i
90	.0868-.5768 i	-.2679-1.2536 i	-.1528-.2254 i	-.5870-.3850 i	.751-.363 i
180	.0395-.6602 i	-.4409-1.4382 i	-.2035-.2362 i	-.7310-.3817 i	.858-.414 i
270	.0868-.5768 i	-.2679-1.2536 i	-.1528-.2254 i	-.5870-.3850 i	.751-.363 i
<u>$k = .5, (\lambda = 1)$</u>					
0°	-.0012-.1970 i	-.2132-.4313 i	-.0548-.0926 i	-.3034-.1828 i	1.678-.477i
90	-.1451-.2644 i	-.7073-.5344 i	-.1750-.0723 i	-.6722-.0372 i	2.907-1.244i
180	-.2243-.3014 i	-.9522-.6159 i	-.2435-.0606 i	-.8755+.0161 i	3.480-1.449i
270	-.1451-.2644 i	-.7073-.5344 i	-.1750-.0723 i	-.6722-.0372 i	2.907-1.244i
<u>$k = .25, (\lambda = .5)$</u>					
0°	-.0416-.0985 i	-.2817-.2159 i	-.0550-.0463 i	-.3042-.0913 i	6.34 -.949i
90	-.2255-.1079 i	-.9035-.1735 i	-.2181+.0041 i	-.8374-.1362 i	15.63-4.56 i
180	-.3157-.1287 i	-1.1718-.2289 i	-.3046+.0138 i	-1.0955+.1665 i	16.18-4.80 i
270	-.2255-.1079 i	-.9035-.1735 i	-.2181+.0041 i	-.8374-.1362 i	15.63-4.56 i
<u>$k = .1, (\lambda = .2)$</u>					
0°	-.0529-.0394 i	-.3009-.0864 i	-.0550-.0185 i	-.3045-.0365 i	39.0-2.37 i
90	-.2697-.0320 i	-1.0425-.0262 i	-.2658+.0199 i	-1.0215+.1250 i	98.9-17.36 i
180	-.3571-.0445 i	-1.2898-.0664 i	-.3533+.0195 i	-1.2703+.1170 i	113.6-15.79 i
270	-.2697-.0320 i	-1.0425-.0262 i	-.2658+.0199 i	-1.0215+.1250 i	98.9-17.36 i

TABLE 3: • CONTINUED

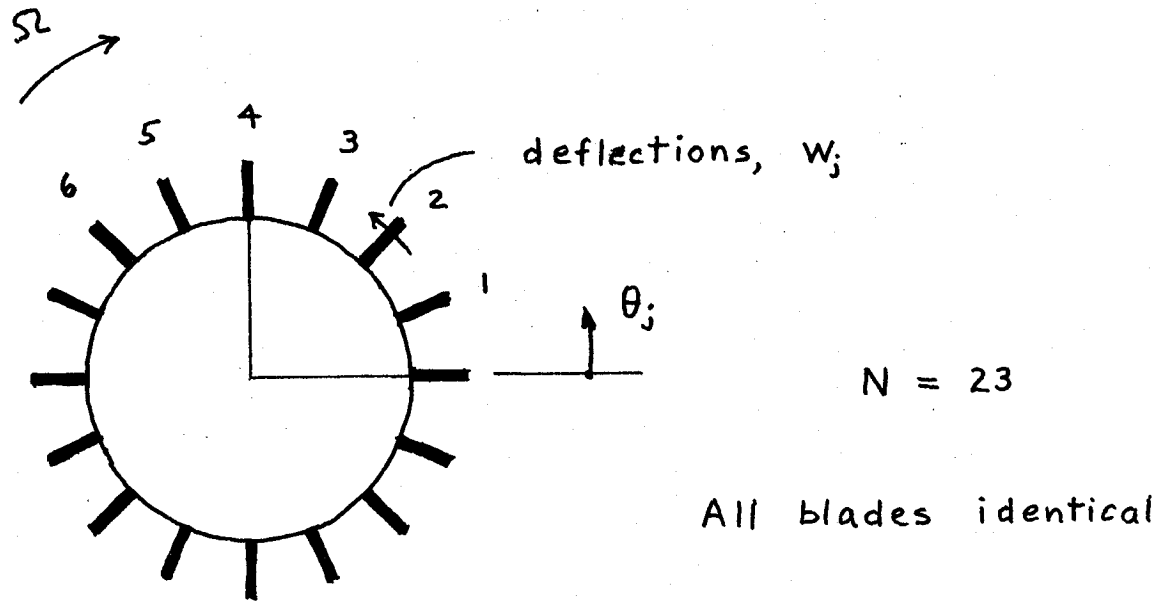
$$s/c = 1, \quad \xi = 45^\circ$$

β	$C_{M\alpha}$	$C_{F\alpha}$	C_{Mq}	C_{Fq}	m_α
<u>$k = 1, (\lambda = 2)$</u>					
0°	.1697-.5045 i	.0266-1.1191 i	-.0912-.2296 i	-.4234-.4547 i	.617-.262 i
90	.0620-.5658 i	-.2705-1.3367 i	-.1661-.2006 i	-.6415-.3861 i	.759-.208 i
180	.0239-.5998 i	-.4596-1.3020 i	-.1875-.2080 i	-.6796-.3180 i	.819-.404 i
270	.1109-.5432 i	-.2243-1.0775 i	-.1218-.2309 i	-.4809-.3592 i	.687-.492 i
<u>$k = .5, (\lambda = 1)$</u>					
0°	-.0266-.2525 i	-.3140-.5611 i	-.0917-.1147 i	-.4261-.2267 i	2.08-.522 i
90	-.1599-.2764 i	-.7253-.7066 i	-.1987-.0671 i	-.7818-.1236 i	3.20-.307 i
180	-.2192-.2797 i	-.9309-.5779 i	-.2334-.0506 i	-.8458+.0345 i	3.40-1.37 i
270	-.1191-.2398 i	-.6193-.3617 i	-.1404-.0731 i	-.5242+.0221 i	2.38-1.92 i
<u>$k = .25, (\lambda = .5)$</u>					
0°	-.0756-.1263 i	-.3989-.2808 i	-.0919-.0573 i	-.4269-.1133 i	7.92-1.04 i
90	-.2292-.1408 i	-.8986-.4302 i	-.2380-.0212 i	-.9300-.0842 i	14.4+1.12 i
180	-.2961-.1282 i	-1.1070-.2466 i	-.2882+.0062 i	-1.0444+.1315 i	15.5-4.06 i
270	-.1968-.0866 i	-.7829+.0079 i	-.1813+.0110 i	-.6638+.2492 i	10.6-8.20 i
<u>$k = .1, (\lambda = .2)$</u>					
0°	-.0894-.0505 i	-.4226-.1123 i	-.0920-.0229 i	-.4271-.0453 i	48.8-2.60 i
90	-.2533-.0740 i	-.9634-.3199 i	-.2589-.0232 i	-.9933-.1730 i	93.8+24.9 i
180	-.3244-.0484 i	-1.1810-.0882 i	-.3220+.0103 i	-1.1669+.0808 i	105.2-12.2 i
270	-.2367-.0064 i	-.8966+.1897 i	-.2274+.0395 i	-.8419+.3126 i	80.0-48.2 i

TABLE 4: VALUES OF m_α FROM THEODORSEN SINGLE AIRFOIL THEORY

$$m_\alpha = \frac{1}{8} + \left[\frac{C(k) - 1}{2k} \right] i + \frac{C(k)}{k^2}$$

k	C(k)	m_α	$\frac{V}{b\omega}$
1	.539 - .100 i	.714 - .331 i	1
.5	.598 - .151 i	2.67 - 1.01 i	2
.25	.693 - .185 i	11.58 - 3.57 i	4
.1	.832 - .172 i	84.2 - 18.0 i	10



Location of j^{th} blade, $\theta_j = \frac{2\pi}{N} j$

FIG. 1: TUNED ROTOR WITH A RIGID DISK

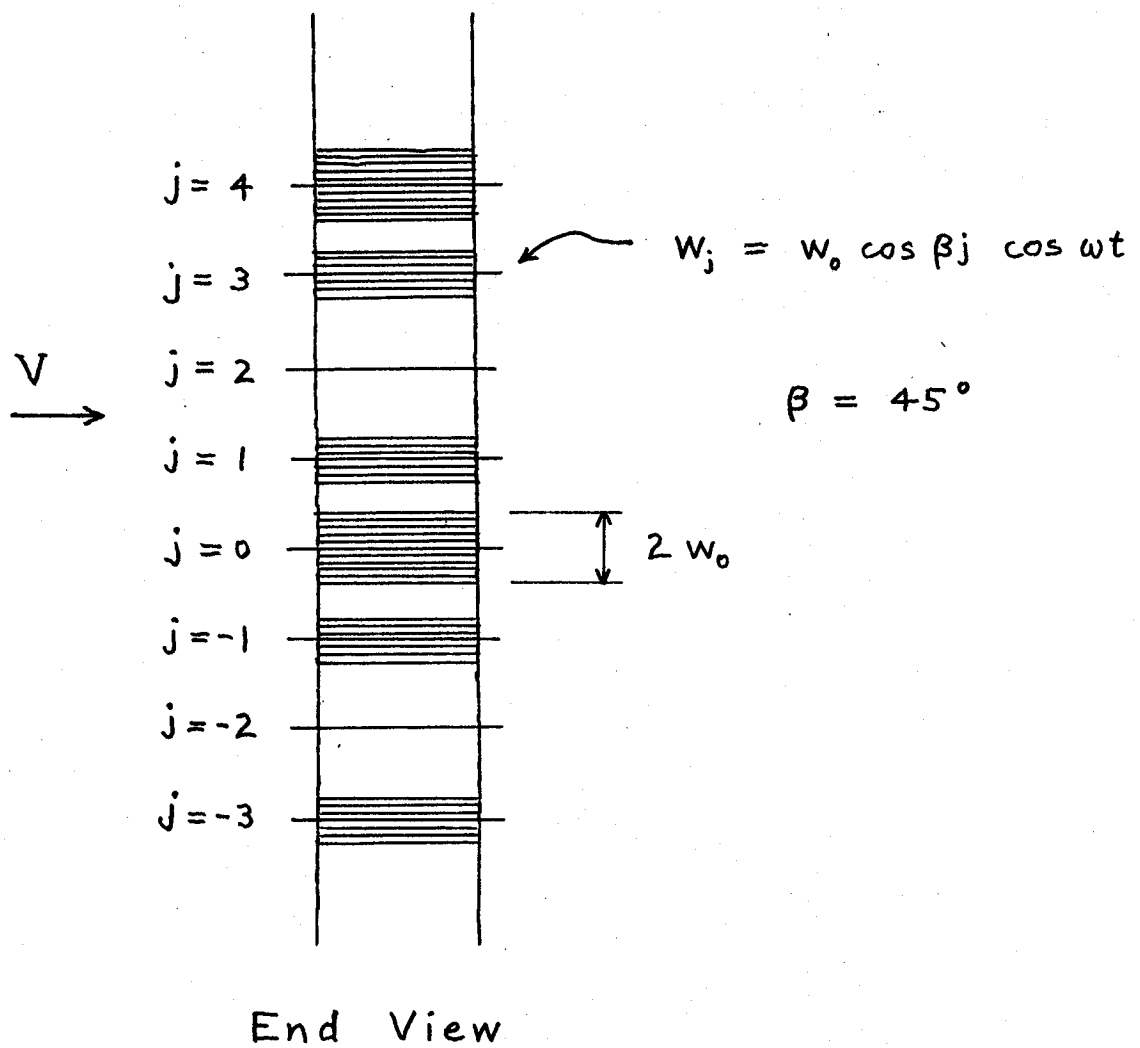
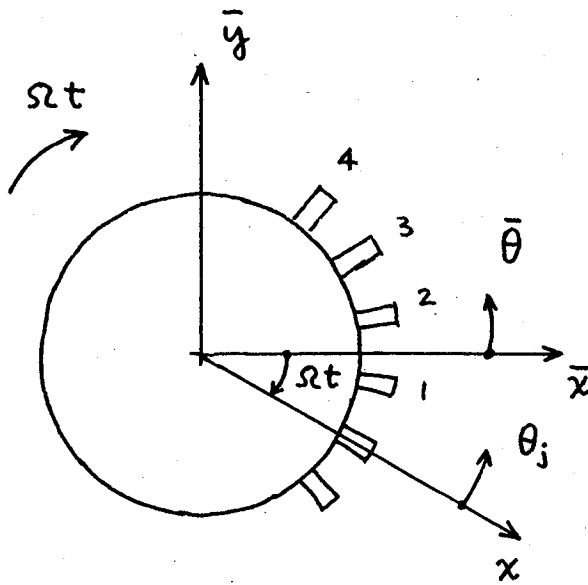


FIG. 2: STANDING WAVE OSCILLATION PATTERN

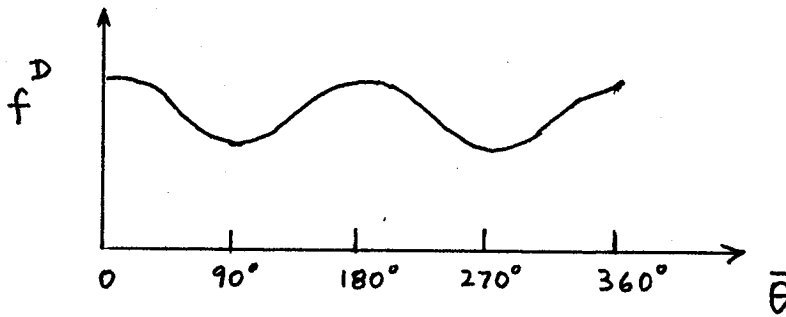


$\bar{x}, \bar{y} \rightarrow$ axes fixed in space

$x \rightarrow$ axis fixed to moving disk

$\bar{\theta} \rightarrow$ angle with respect to fixed space

$\theta_j = \frac{2\pi}{N} j \rightarrow$ location of blade j



$$f^D(\bar{\theta}) = f_{cm} \cos m\bar{\theta} + f_{sm} \sin m\bar{\theta}$$

$$\begin{aligned} f_j^D &= f_{cm} \cos m(\theta_j - \Omega t) + f_{sm} \sin m(\theta_j - \Omega t) \\ &= \left(f_{cm} \cos m \frac{2\pi}{N} j + f_{sm} \sin m \frac{2\pi}{N} j \right) \cos m\Omega t \\ &\quad + \left(f_{cm} \sin m \frac{2\pi}{N} j - f_{sm} \cos m \frac{2\pi}{N} j \right) \sin m\Omega t \end{aligned}$$

FIG. 3: FORCED EXCITATION OF ROTOR DISK

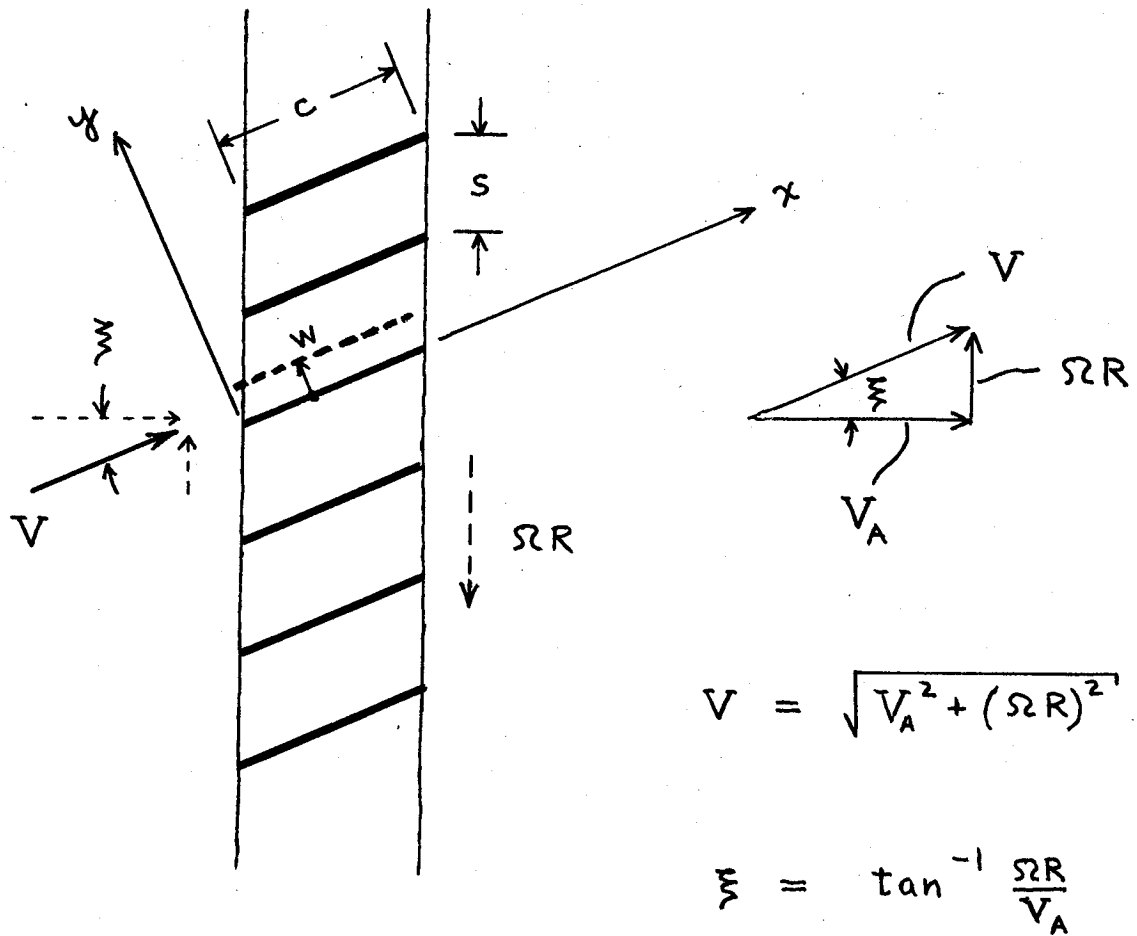


FIG. 4: GEOMETRICAL LAYOUT FOR BENDING FLUTTER

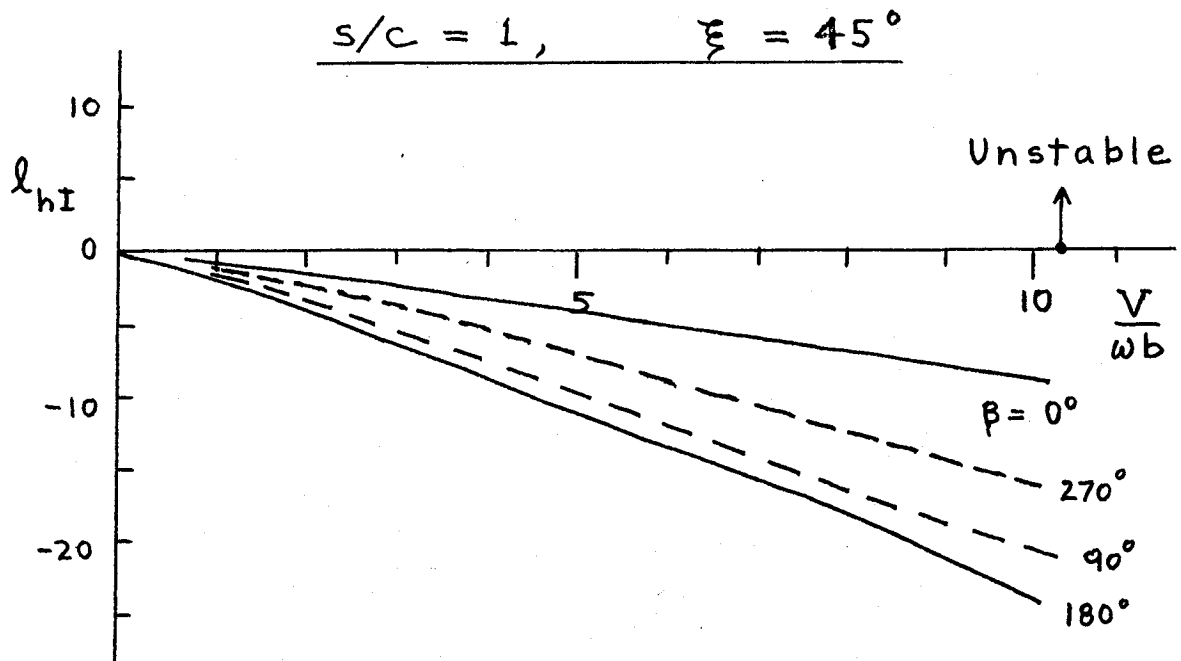
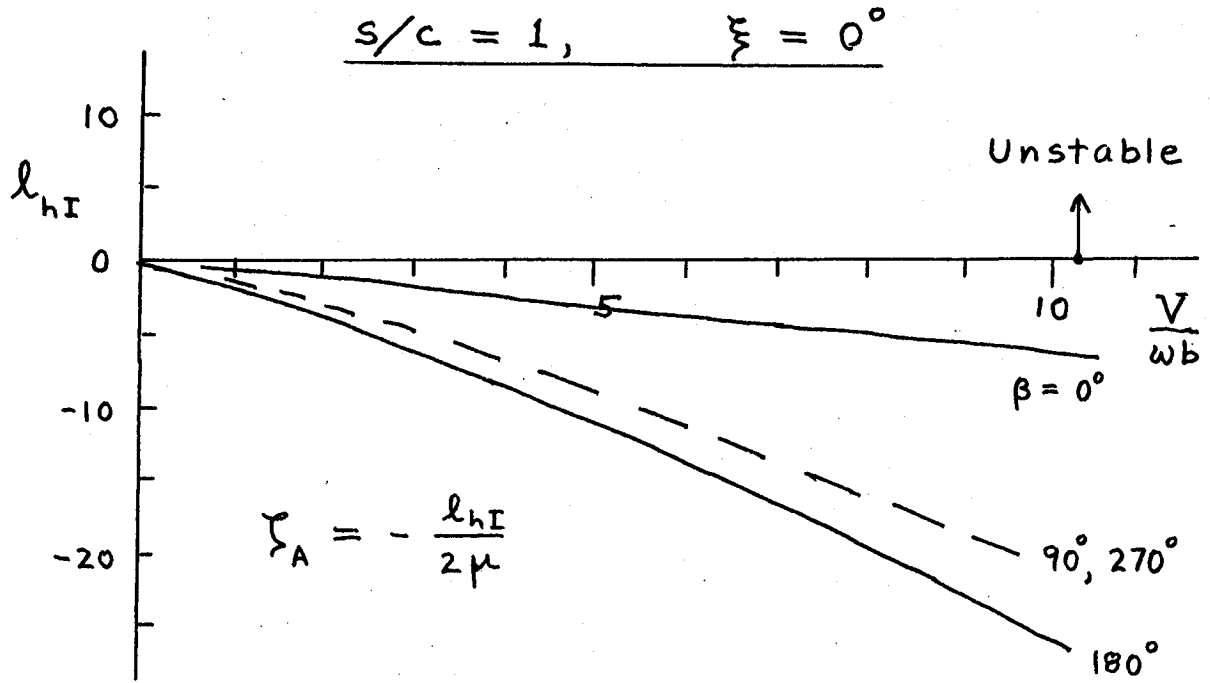


FIG. 5: AERODYNAMIC DAMPING VALUES FOR BENDING FLUTTER

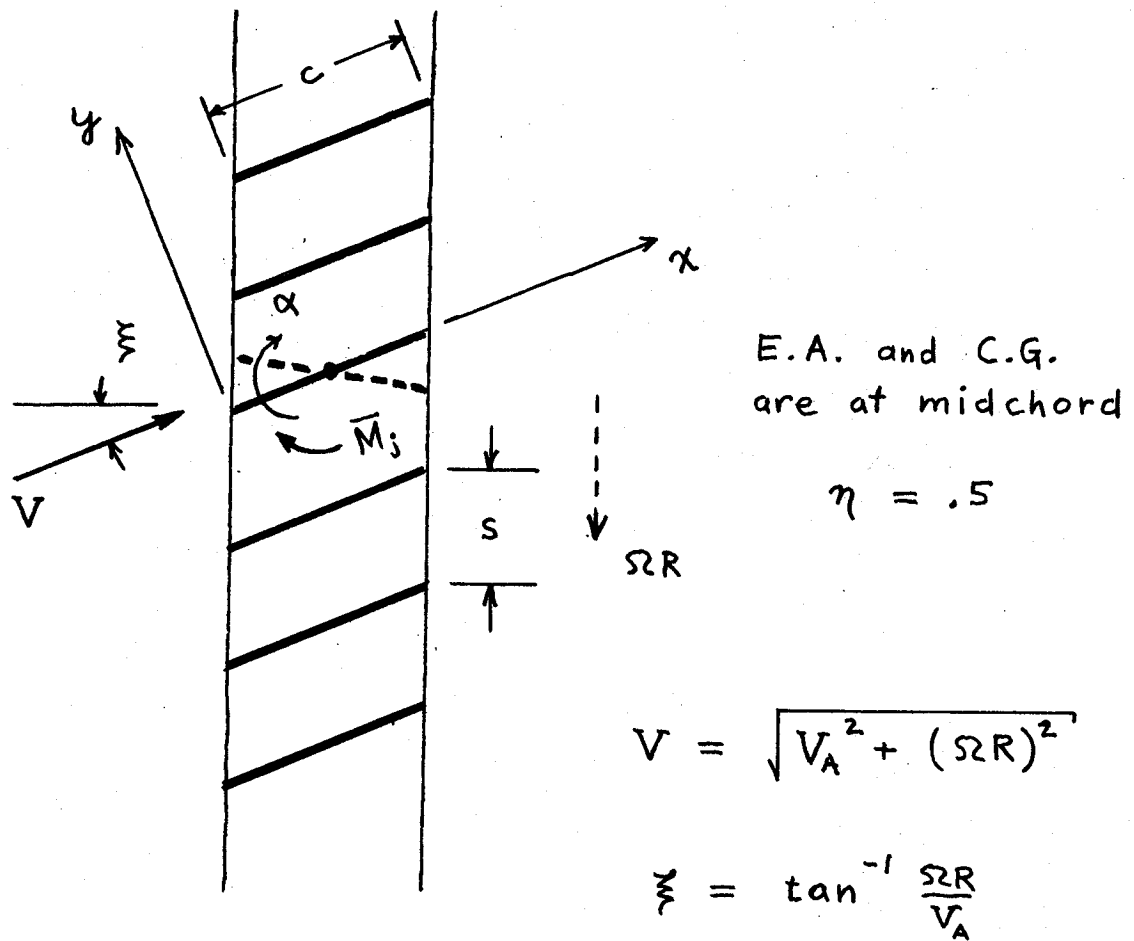


FIG. 6: GEOMETRICAL LAYOUT FOR TORSION FLUTTER

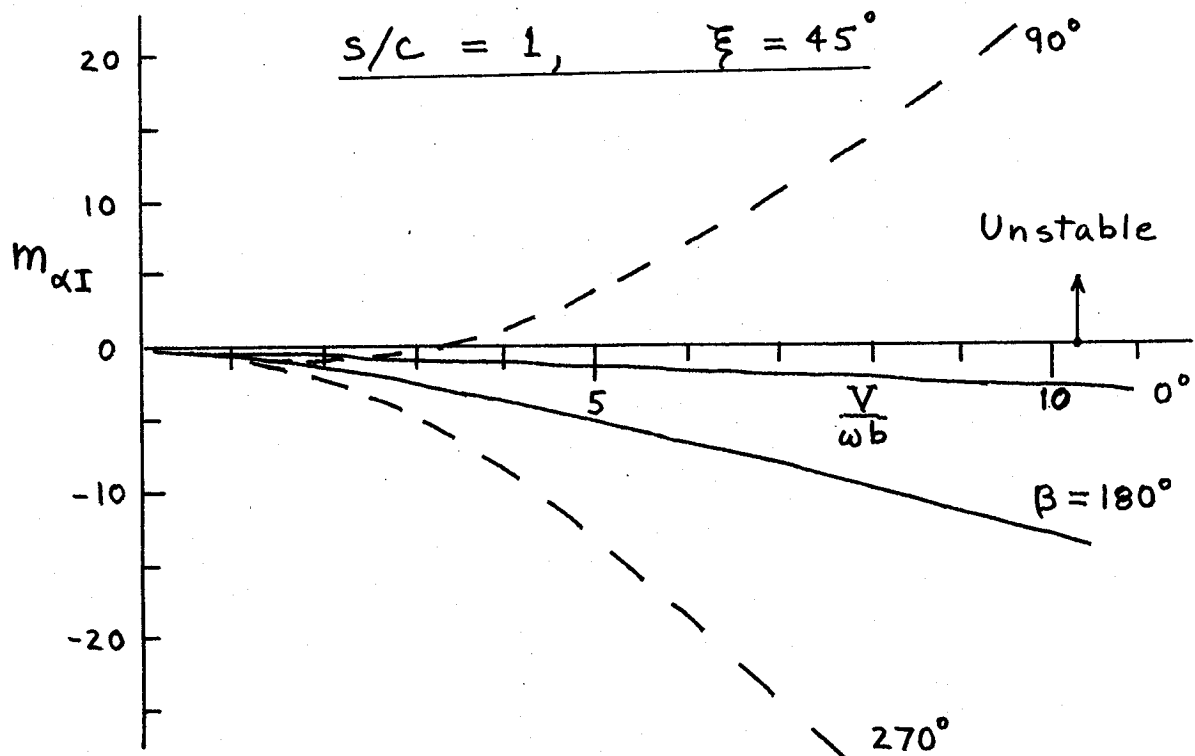
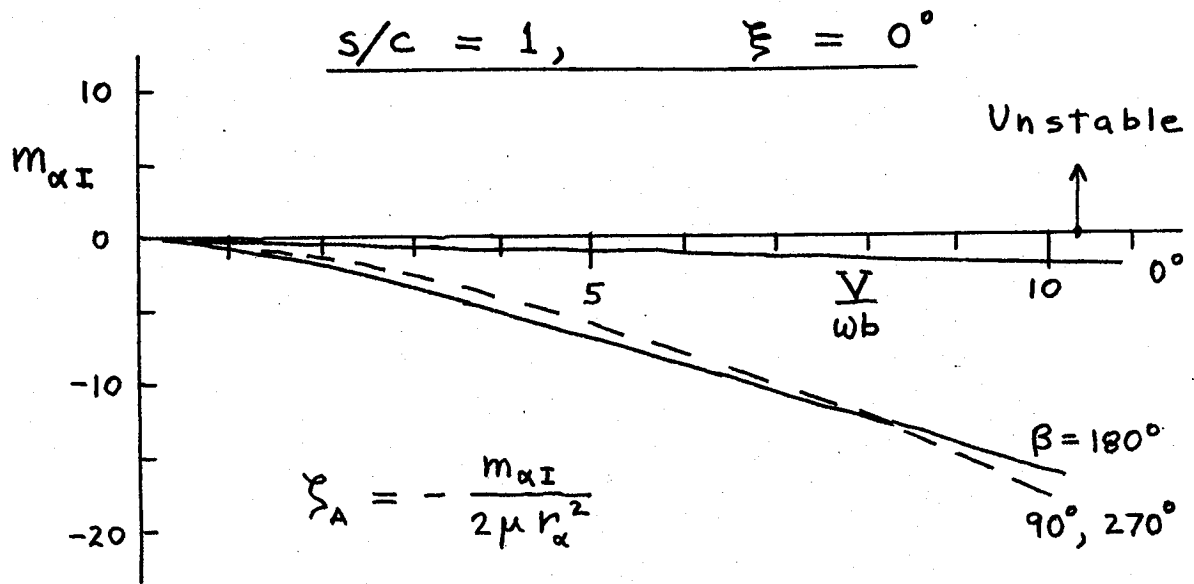
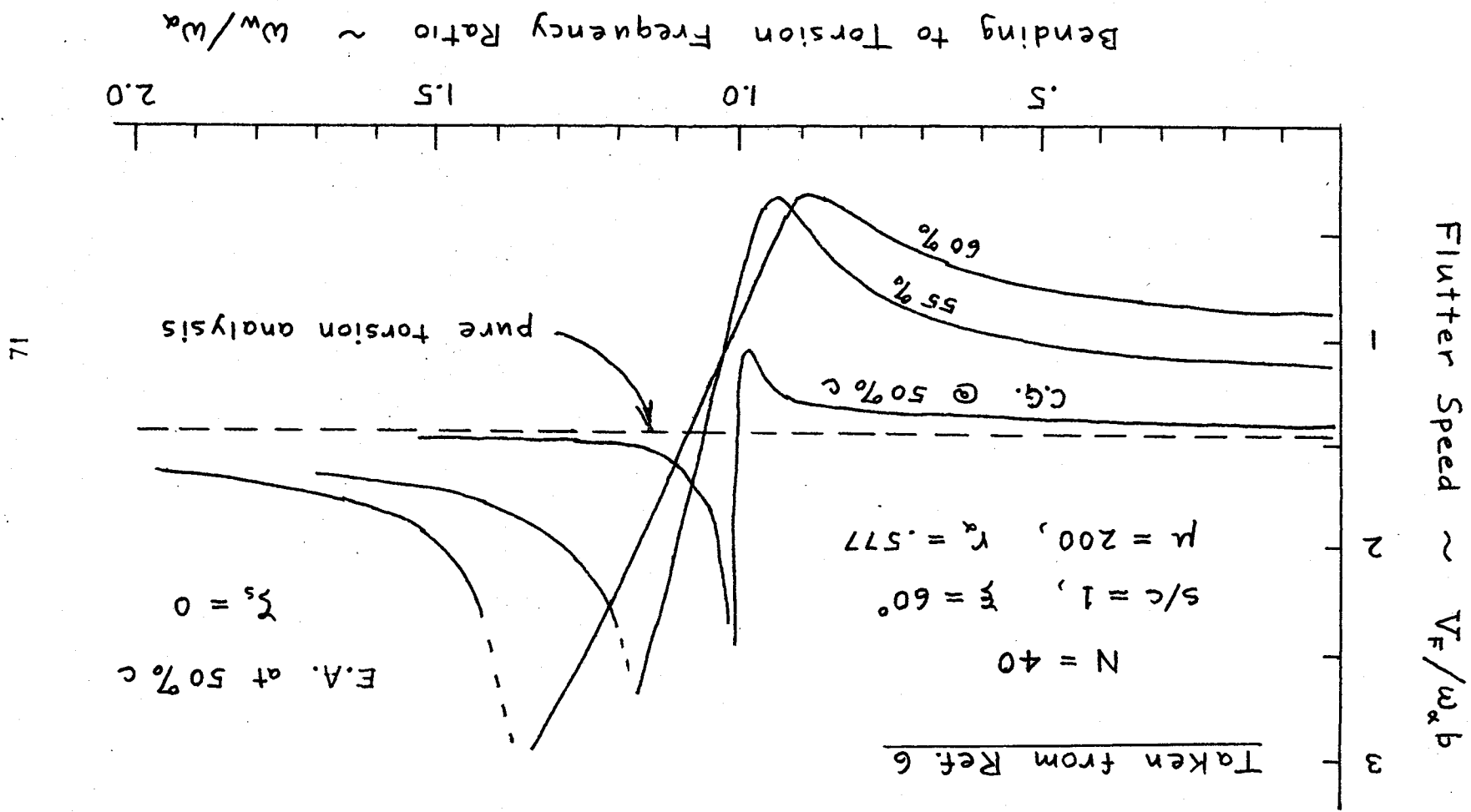
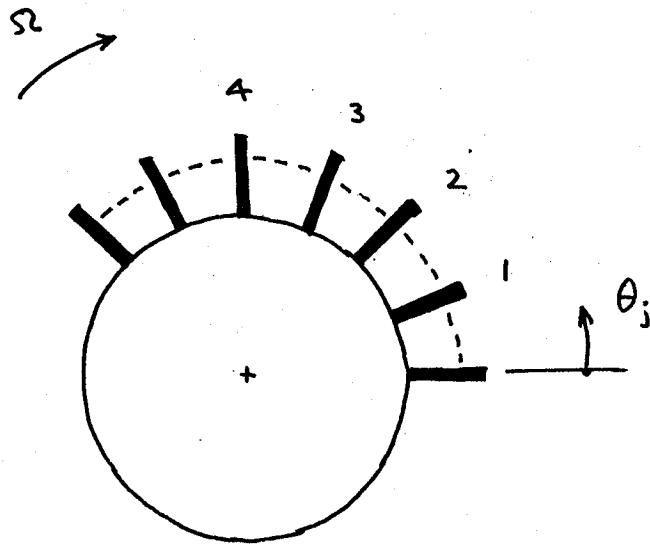


FIG. 7: AERODYNAMIC DAMPING VALUES FOR TORSION FLUTTER

FIG. 8: FLUTTER SPEEDS FOR COMBINED BENDING-TORSION FLUTTER





$$N = 23$$

All blades identical

Location of j^{th} blade, $\theta_j = \frac{2\pi}{N} j$

FIG. 9: TUNED ROTOR WITH FLEXIBLE DISK

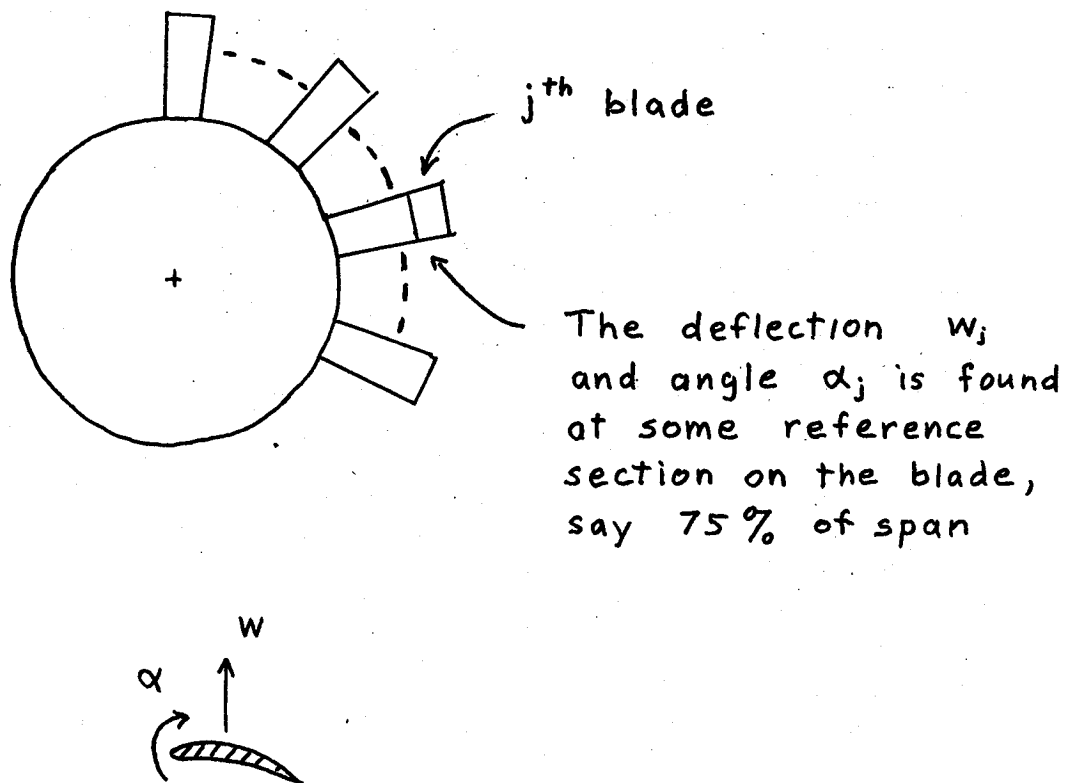
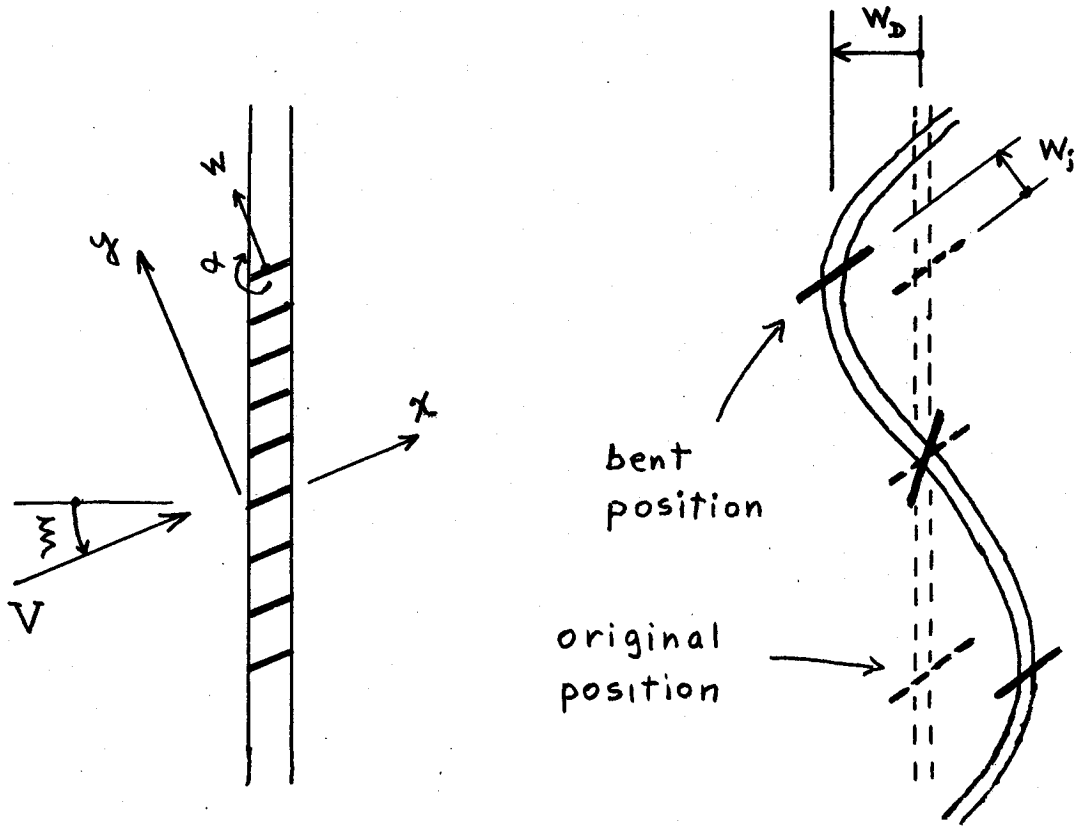


FIG. 10: DESCRIPTION OF j^{th} BLADE OF ROTOR ASSEMBLY



$$\text{Disk mode} = w_D \cos n\theta$$

$$\text{At blade location, } n\theta_j = n \frac{2\pi}{N} j = \beta_j ,$$

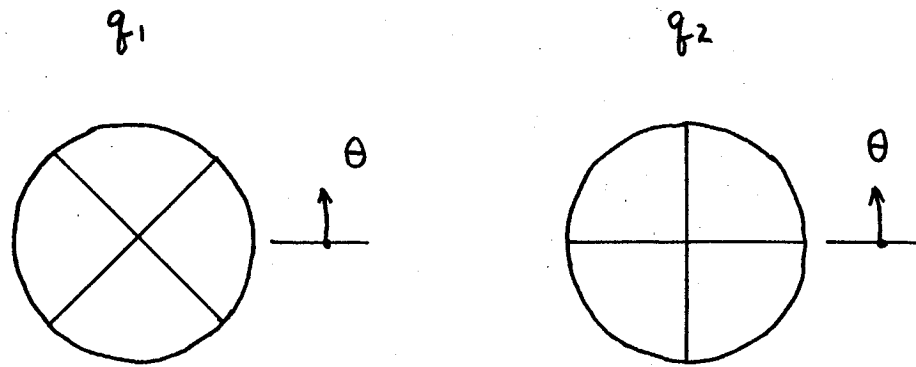
$$w_j \text{ deflection} = (w_D \sin \xi + w_B) \cos \beta_j$$

$$\begin{aligned} \alpha_j \text{ angle} &= \left(\frac{1}{R} \frac{dw_D}{d\theta} + \alpha_B \right) \sin \beta_j \\ &= \left(-\frac{w_D}{R} n + \alpha_B \right) \sin \beta_j \end{aligned}$$

FIG. 11: BLADE DEFLECTIONS FOR FLEXIBLE ROTOR DISKS

$n = 2$ mode

$$n\theta_j = n \frac{2\pi}{N} j = \beta_j$$



$$w_j = bh_0 \cos \beta_j$$

$$\begin{aligned} w_j &= bh_0 \cos(\beta_j - 90^\circ) \\ &= bh_0 \sin \beta_j \end{aligned}$$

The two modes are shifted by 90°

FIG. 12: SYMMETRY RELATIONS FOR STANDING WAVE MODES

